An Analysis of Regional Climate Simulations for Western Australia's Wine Regions—Model Evaluation and Future Climate Projections

REBECCA FIRTH, JATIN KALA, THOMAS J. LYONS, AND JULIA ANDRYS

Environmental and Conservation Sciences, School of Veterinary and Life Sciences, Murdoch University, Murdoch, Western Australia, Australia

(Manuscript received 6 October 2016, in final form 16 May 2017)

ABSTRACT

The Weather Research and Forecasting (WRF) Model is evaluated as a regional climate model for the simulation of climate indices that are relevant to viticulture in Western Australia's wine regions at a 5-km resolution under current and future climate. WRF is driven with ERA-Interim reanalysis for the current climate and three global climate models (GCMs) for both current and future climate. The focus of the analysis is on a selection of climate indices that are commonly used in climate–viticulture research. Simulations of current climate are evaluated against an observational dataset to quantify model errors over the 1981–2010 period. Changes to the indices under future climate based on the SRES A2 emissions scenario are then assessed through an analysis of future (2030–59) minus present (1970–99) climate. Results show that when WRF is driven with ERA-Interim there is generally good agreement with observations for all of the indices although there is a noticeable negative bias for the simulation of precipitation. The results for the GCM-forced simulations were less consistent. Namely, while the GCM-forced simulations performed reasonably well for the temperature indices, all simulations performed inconsistently for the precipitation index. Climate projections showed significant warming for both of the temperature indices and indicated potential risks to Western Australia's wine growing regions under future climate, particularly in the north. There was disagreement between simulations with regard to the projections of the precipitation indices and hence greater uncertainty as to how these will be characterized under future climate.

1. Introduction

The grapevine is particularly sensitive to its environment and has well-defined climatic conditions that enable it to grow and ripen its fruit to an optimum level (Urhausen et al. 2011). Growing wine grapes outside of their optimum climatic thresholds can detrimentally impact the resulting wine quality. Accordingly, centuries of experience have enabled the suitable pairing of premium wine varieties with their most favorable environments (Moriondo et al. 2013). This has resulted in the world's viticulture regions for high-quality wine production being associated with fairly narrow geographical and therefore climatic niches that inevitably place them at particular risk from climate change (Jones 2007). Several studies have investigated the effects of climate change on wine grape production. It has been shown that hotter growing conditions can cause negative effects for wine grape color and acidity (Barnuud et al. 2014a,b) as well as an increase in alcohol content (Duchêne and Schneider 2005; Jones and Goodrich 2008). Warmer and drier conditions have also been associated with significant advancements in the timing of phenological events, such as budburst and harvest, and decreases in wine grape yield (Fraga et al. 2016). Furthermore, it has been indicated that some regions in the south of Europe will become climatically unsuitable to produce high-quality wine, while previously unsuitable northern regions will become viable under a range of future climate scenarios (Tóth and Végvári 2016).

Western Australia (WA) supports an industry for world-class wine production that makes a significant contribution to the state's economy. For example, in 2010, viticulture represented 41% of the total value (AUD $1.1 billion) added by horticulture to WA's economy (Wines of Western Australia 2014). Viticulture in WA makes up less than 5% of the total production by volume nationally, yet it represents almost 25% of Australia's premium wine market (Wines of Western Australia 2014). Therefore, wine quality is

Corresponding author: Jatin Kala, j.kala@murdoch.edu.au

DOI: 10.1175/JAMC-D-16-0333.1

particularly important to WA's wine industry in terms of its monetary value as well as its identity. The state's wine grape growing regions are predominantly located in its southwestern corner, an area of known vulnerability to climate change, with significant trends toward a warmer and drier climate (Hope 2006; Bates et al. 2008).

Prior research into climate change in WA's wine regions has indicated that the region may face challenges under future climate. However, these studies have largely relied upon climatic data provided by global climate models (GCMs), which are limited in their applicability to viticulture research because of their coarse resolution of 100–250 km. For example, Hall and Jones (2009) evaluated climate projections from a single GCM to investigate how several temperature indices that describe Australia's wine grape growing conditions may change under future climate. The study focused on all of Australia's wine regions and included an analysis of WA. Their findings indicated that temperatures will increase in WA's wine regions and that these increases could result in some regions no longer being viable for premium wine production, particularly the state's northern regions.

In two national studies that also included evaluations of WA's wine regions, Webb et al. (2007, 2008) used GCMs to investigate climate change impacts on wine grape quality and grapevine phenology, respectively. Their findings indicated that a warmer climate would result in changes to the timing of phenological events for the grapevine in WA's wine regions. Projected changes included a shorter growing season and the delayed occurrence of budburst (Webb et al. 2007). A reduction in wine grape quality, particularly in the state's northern wine regions, was also projected (Webb et al. 2008). While these GCM-based studies provide highly valuable information about the potential impacts of climate change on viticulture in WA, they are nonetheless inherently limited by their coarse resolution. GCMs are well documented to be unable to resolve finescale features, including topography, land cover, and mesoscale weather systems (e.g., Christensen et al. 2007; Rummukainen 2016). Additionally, the wine-producing region of WA is located in the southwest, which is a region of strong land–atmosphere coupling (Hirsch et al. 2014b), and being situated close to the coast, it frequently experiences sea breezes (Clarke 1989). Hence, there is potential for regional climate models (RCMs) to add value to GCMs in the region, and this has been shown by recent studies (Andrys et al. 2015, 2016).

Given the issues associated with the coarse resolution of GCMs, some studies have used the "statistical downscaling" technique to downscale future climate projections from GCMs to provide regional climate information for WA's wine regions (Barnuud 2012). While this approach can be useful because of its low computational cost, it is based on the assumption that present-day relationships between large- and local-scale climate will remain the same under future climate, which is nonverifiable (Hewitson et al. 2014; Wilby et al. 2004). Additionally, these simulations do not provide information on changes in the dynamics of the atmosphere, and given the known effects of topography (Pitts and Lyons 1990), land use (Hirsch et al. 2014b,a), and mesoscale features such as the sea breeze (Clarke 1989) in the region, there is clearly a need for high-resolution regional climate projections for WA's wine regions, which are not provided by GCMs or statistical downscaling approaches. Additionally, prior research has shown the benefits of using RCMs to provide climatic information for viticultural regions elsewhere, including France (Xu et al. 2012; Bonnefoy 2013; Bonnardot et al. 2014) and South Africa (Bonnardot and Cautenet 2009).

RCM simulations for southwest Western Australia (SWWA), which includes all the wine-producing regions of WA (Fig. 1), have been conducted by Kala et al. (2015) and Andrys et al. (2015, 2016, 2017) using the Weather Research and Forecasting (WRF) Model. WRF is a next-generation mesoscale modeling system (Skamarock et al. 2005) that has been commonly used for the purposes of dynamically downscaling GCMs, including applications in Europe (Heikkilä et al. 2011; Soares et al. 2012), North America (Gula and Peltier 2012), Asia (Chotamonsak et al. 2011; En-Tao et al. 2010), and eastern Australia (Evans and McCabe 2010). WRF is also one of the RCMs that is being used for the Coordinated Regional Climate Downscaling Experiment (CORDEX; Giorgi et al. 2009), an international initiative of the World Climate Research Program.

WRF, like any RCM, is sensitive to model physics options as well as the input forcing data, and this sensitivity was assessed by Kala et al. (2015) over SWWA at a 10-km resolution over a 1-yr time scale. They found that the ERA-Interim (Dee et al. 2011) was the best-performing reanalysis for the region as compared with the NCEP–NCAR reanalysis (Kalnay et al. 1996) and NCEP's final (FNL) global tropospheric reanalysis, and they also determined the best combination of WRF physics options (among some of the most commonly used options) for SWWA. This study found that generally, WRF simulated the climate of SWWA well. However, issues were highlighted relating to the model's inability to adequately reproduce summer rainfall and an underestimation of coastal rainfall, which was attributed to unresolved topography at a 10-km resolution.

Based on the findings of Kala et al. (2015), Andrys et al. (2015) used the same model setup of Kala et al. (2015) but

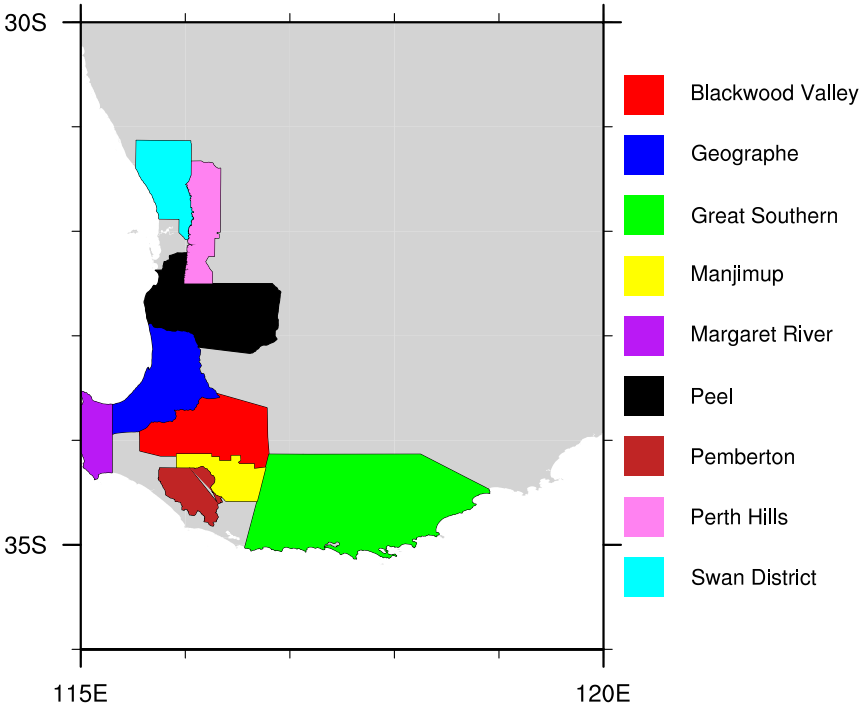

FIG. 1. Western Australia's wine regions.

extended the simulations over a 30-yr period (1981–2010) using ERA-Interim. Two nested domains at 5- and 10-km resolutions were evaluated. Their study focused on climate extremes and indices that are of significance to cereal crop applications. The higher-resolution simulation showed improved skill in reproducing summer and autumn rainfall and rainfall on the midwest coast owing to an improved resolution of the topography. Warm and cold extremes and seasonal minimum and maximum temperatures were well represented by WRF; however, there was a tendency to underestimate average maximum temperatures and overestimate average minimum temperatures.

While the work of Andrys et al. (2015) provided a very useful climatology for SWWA, the use of a reanalysis to drive the simulations restricts the analysis to the present climate only. Therefore, Andrys et al. (2016) conducted further research to investigate WRF's skill in reproducing the historical climate of SWWA at a 5-km resolution when driven with four different GCMs. The focus was on the simulation of winter cold fronts that bring the bulk of the rainfall to the region and climate extremes during the cereal crop growing season. Results were varied between the four GCM-forced simulations, with one of them performing exceptionally well in reproducing the climatology of SWWA, two reasonably well, and one poorly. Issues that were highlighted were attributed to both systematic errors present in WRF and the lateral boundary conditions provided by the GCMs. WRF was shown to add value to the GCMs when simulating the daily distribution of rainfall, particularly during the cereal crop growing season. However, it was found that WRF consistently simulated cooler temperatures than the GCMs and demonstrated significant biases for maximum temperatures in some simulations.

Following on from assessing the biases in WRF and the four GCMs, Andrys et al. (2017) analyzed WRF projections of SWWA climate driven by three GCMs for the period 2030–59 relative to 1970–99. They investigated changes to the distribution of daily temperatures, seasonal means, and extreme climate indices relevant to cereal crops. Their findings indicated that temperatures would increase and that this would be most pronounced for maximum temperatures in comparison with minimum temperatures. All simulations agreed that winter precipitation would decrease; however, the magnitude of the projected decrease varied between simulations. There was less model agreement with regard to changes in precipitation for the other seasons.

In summary, SWWA is a region of significant wine production. Previous studies have predominantly relied on GCMs alone (Webb et al. 2007, 2008; Hall and Jones 2009) or statistical downscaling (Barnuud 2012) to investigate future changes in climate with respect to wine production. The recent work of Andrys et al. (2015, 2016, 2017) using WRF as an RCM to provide regional climate projections for the region provides a valuable

opportunity to investigate the impacts of future climate change on the viticulture industry. The aim of this paper is to first evaluate WRF as an RCM to be used for future climate–viticulture research in SWWA by focusing on indices that are relevant to viticulture and, second, to assess the future risks associated with viticulture in this region. The first aim will be addressed by comparing outputs from WRF driven with boundary conditions from reanalysis data (Andrys et al. 2015) with an observational dataset for the present climate over a 30-yr period. This will involve examining long-term means as well as time series and will quantify the biases inherent in WRF. Following this, an evaluation of WRF climate simulations under current climate using boundary conditions from three GCMs (Andrys et al. 2016) will be carried out through a comparison with the observational dataset. This analysis will be limited to long-term means only and will highlight the limitations of the GCMs. Finally, with an understanding of the biases inherent in WRF and the GCMs, projections of the climate indices relevant to viticulture will be analyzed to quantify changes to the growing conditions for viticulture in SWWA under future climate.

2. Methods

a. SWWA

There are nine wine-producing regions in WA, as shown in Fig. 1. These regions are located predominantly in the state's southwest. SWWA experiences a Mediterranean-type climate that is characterized by hot, dry summers and cool, wet winters (Charles et al. 2010; Gentilli 1972). Over 80% of the annual rainfall falls during the cooler months (May–October). There is a strong decrease in the rate of rainfall from south to north across the region and a slight increase over the first 30 km from west to east. This increase in rainfall is most prominent around the Darling Scarp; whereafter, the rate of rainfall decreases with distance inland (Wright 1974). The Darling Scarp is a 300-m-high escarpment located 25 km inland running parallel to the north–south coastline and can be seen in Fig. 2b. Andrys et al. (2015) showed that WRF simulations at 10-km resolution had a positive bias on the windward (west) side of the scarp and strong negative bias east of the scarp. Simulations at 5-km resolution resolved the positive bias and reduced the negative bias, but nonetheless, a lower negative bias remained east of the scarp, which would potentially have an impact on wine regions along the west coast (Fig. 1).

WA's wine regions are currently most reputable for the production of premium white grape varieties, including chardonnay, semillon, and sauvignon blanc in Margaret River, riesling in the Great Southern; and verdelho in the Swan District. The Margaret River region is also renowned for the production of premium red grape varieties, specifically, cabernet sauvignon and merlot. The growing season for wine grapes occurs in the warmer months from 1 October to 30 April.

b. Climate model data

The RCM data analyzed in this study were produced by Andrys et al. (2015, 2016, 2017) using WRF, version 3.3 (Skamarock et al. 2005). Three nested domains were used as illustrated in Fig. 2. The outer domain was at a 50-km resolution based on the CORDEX Australasia domain and the two nested domains at 10- and 5-km resolutions, respectively. A 3-month model spinup period was used. The model setup and parameter options that were chosen by Andrys et al. (2015, 2016, 2017) were based on the findings of Kala et al. (2015), who explored the sensitivity of WRF to different physics options and input forcing data over SWWA. The setup included the single-moment 5-class microphysics scheme (Hong et al. 2004), the Rapid Radiative Transfer Model for longwave radiation (Mlawer et al. 1997), the Dudhia scheme for shortwave radiation (Dudhia 1989), the Yonsei University planetary boundary layer scheme (Hong and Lim 2006), the Kain–Fritsch (Kain 2004) scheme for convective parameterization for the first (50 km) and second (10 km) domains only, the MM5 surface-layer scheme (Grell et al. 2000), and the Noah land surface model (Chen and Dudhia 2001). The model used a 150-day averaging period for deep soil temperatures and spectral nudging above the planetary boundary layer for the outer domain only. Thirty vertical levels were used, with levels more tightly packed close to the surface to ensure higher resolution close to the ground. Carbon dioxide concentrations were updated monthly based on observations from Baring Head, New Zealand (Keeling et al. 2001), considered to be representative of the Southern Hemisphere. Before analyzing the results, a 10-gridpoint relaxation zone was removed from the domain boundaries to account for the relaxation zone.

The innermost nested domain (5-km resolution) was chosen for evaluation in this study as it was shown by Andrys et al. (2015) to provide a superior representation of SWWA climate. The climate simulations for SWWA were driven with boundary conditions from ERA-Interim (section 1) and three GCMs (section 2). ERA-Interim-driven simulations were available for the period 1981–2010 (Andrys et al. 2015), and the GCM-forced simulations were available for the periods 1970–99 for current climate (Andrys et al. 2016) and 2030–59 for future climate (Andrys et al. 2017).

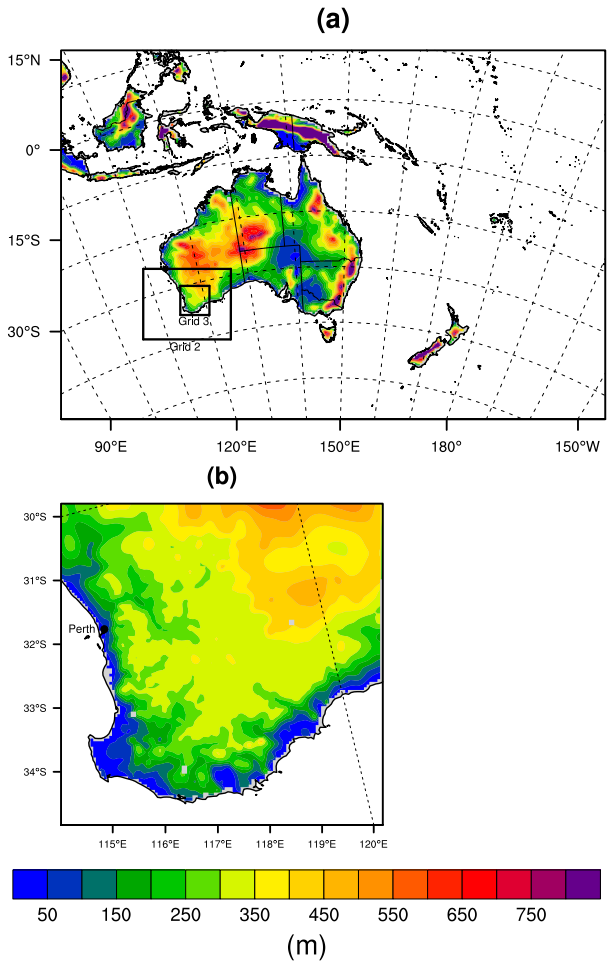

FIG. 2. Contour map showing the topography of (a) the outer model domain (50-km resolution), including the extent of the nested grids, and (b) the topography of the innermost nested domain (5-km resolution) used by Andrys et al. (2015, 2016, 2017) in the WRF simulations of present and future climate (Andrys et al. 2015).

1) ERA-INTERIM

ERA-Interim is a reanalysis produced from the European Centre for Medium-Range Weather Forecasts. It is available beginning in 1979 and continues to be updated in real time with a 6-h analysis window. It has a spatial resolution of approximately 80 km, and there are 60 vertical levels from the surface up to 0.1 hPa. The ERA-Interim-forced simulation will now be referred to as WRF-ERA.

2) GCMS

The GCMs that have provided the lateral boundary conditions for the WRF simulations of current and future climate are the National Center for Atmospheric Research Community Climate System Model, version 3 (CCSM3; Collins et al. 2006); the Commonwealth Scientific and Industrial Research Organization Mark 3.5 (CSIRO; Gordon et al. 2002); and the Max Planck Institute ECHAM5 model (Roeckner et al. 2003). These GCMs are part of phase 3 of the Coupled Model Intercomparison Project (CMIP3), which is the model ensemble that was used to inform the IPCC Fourth Assessment report.

The choice of GCMs by Andrys et al. (2016) was driven by the availability of 6-hourly data from different CMIP3 GCMs at the time and the findings of Perkins et al. (2007), who assessed the performance of several CMIP3 GCMs in simulating temperature and precipitation over Australia and found that these three GCMs performed satisfactorily. Andrys et al. (2016) also included the Model for Interdisciplinary Research on Climate, version 3.2 (MIROC3.2; Hasumi and Emori 2004) in their analysis. However, this model was shown to have a poor performance in simulating the climate of SWWA and has therefore not been included for evaluation in this study.

For all climate projections, the A2 scenario was used. The A2 scenario is at the upper end of the emissions scenarios and postulates little change in greenhouse gas (GHG) emissions over the course of the twenty-first century (Nakićenović and Coauthors 2000). The WRF simulations that have been driven with boundary conditions from CCSM3, CSIRO, and ECHAM5 will be referred to as WRF-CCS, WRF-CSI, and WRF-ECH, respectively.

c. *Observational data*

The observational data used for evaluation consisted of daily gridded observations of precipitation and maximum and minimum temperatures at a resolution of 5 km from 1980 to 2010. These data have been provided by the Australian Bureau of Meteorology (BoM) as part of the Australian Soil Water Availability Project (AWAP; Raupach et al. 2009) and are an interpolation of direct surface measurements recorded from a network of weather stations across Australia. The number of stations recording data varies in time and by variable. Precipitation has been interpolated from between 5000 and 7000 stations across Australia, whereas temperature has only been recorded at between 600 and 850 stations (Jones et al. 2007). The AWAP dataset is currently the best available gridded temperature and precipitation dataset for Australia and has been used for model evaluation purposes by numerous studies (Evans and McCabe 2010; Andrys et al. 2015; Kala et al. 2015). King et al. (2013) evaluated the efficacy of the AWAP dataset in terms of representing extreme rainfall over Australia and demonstrated good agreement with station observations but cautioned against the use of the gridded AWAP dataset in regions with poor station coverage, such as inland central Western Australia.

The wine regions of SWWA are located close to the coast where station density is highest (Jones et al. 2007); hence, this is not an issue.

d. Climate indices

Two temperature indices, the Huglin index (HI) and the cool night index (CI), were selected for analysis. These indices were included in the multicriteria climatic classification (MCC) system developed by Tonietto and Carbonneau (2004) as a research tool for viticultural zoning worldwide. Growing-season precipitation (GSP) was selected to represent the water component in the relationship between climate and viticulture. The gridded observational dataset (Jones et al. 2007; Raupach et al. 2009) provides daily minimum and maximum temperatures. Averages were therefore calculated as the mean of the maximum and minimum temperature. Similarly, averages for all modeled data were calculated as the mean of the daily minimum and maximum temperature to enable comparison. All temperature indices are calculated from the air temperature recorded at 2 m above ground. The class limits for each of the temperature indices, the time frame over which they are calculated, and their main sources are summarized in Table 1.

1) HUGLIN INDEX

The HI [Eq. (1); Huglin 1978] is a heat summation index that is commonly used to describe varietal suitability within a given region. It takes the mean of the average and maximum temperatures, effectively giving an estimate of daytime temperatures. It therefore gives focus to the time of day during which photosynthesis is most active, indicating the sugar potential according to different varieties (Huglin 1978). A base temperature of 10°C is used, and temperatures above this threshold are summed over a 6-month period from October to March (in the Southern Hemisphere). It also includes an adjustment for latitude K to account for varying day lengths (Table 1):

$$\mathrm{HI} = \sum_{1\,\mathrm{Oct}}^{31\,\mathrm{Mar}} \max[(T_{\mathrm{mean}} - 10 + T_{\mathrm{max}} - 10)/2, 0]K, \qquad (1)$$

where K is a latitude coefficient that takes into account increasing day lengths (Table 2).

2) COOL NIGHT INDEX

The CI [Eq. (2)], is calculated as the average minimum temperature of March (in the Southern Hemisphere), which represents the ripening month in the Southern Hemisphere. Minimum temperatures during the ripening period influence wine grape characteristics with respect to color and aroma (Tonietto and Carbonneau 2004). Combined with HI, these indices allow a concise determination of a region's varietal suitability based on the heat accumulation during the vegetative growth period of the vine and nighttime temperatures during the ripening period (Table 1):

$$\mathrm{CI} = \mathrm{avg}(T_{\mathrm{min\_March}}). \qquad (2)$$

3) GROWING-SEASON PRECIPITATION

GSP [Eq. (3)] is an important index for climate–viticulture research for several reasons. First, excessive moisture during this period can provide favorable conditions for diseases such as powdery mildew to develop (Nicholas et al. 1994). It has therefore commonly been used in viticulture–climate evaluations (Cabré et al. 2016; Fraga et al. 2012, 2014). Second, it is used in the calculation of the dryness index, which is the third index included by Tonietto and Carbonneau (2004) in the MCC system and is used to describe the water component of viticulture regions. It is calculated as the total rainfall from October to April (in the Southern Hemisphere):

$$\mathrm{GSP} = \sum_{1\,\mathrm{Oct}}^{30\,\mathrm{Apr}} \mathrm{Precipitation}. \qquad (3)$$

GSP was selected as an index for evaluation in this study because observed (OBS) daily precipitation data were available to allow a comparison with simulations. However, it is a simple index that provides limited information regarding water availability for the grapevine. A more useful index commonly used within the climate sciences is precipitation minus evapotranspiration, as it provides information on the actual amount of soil water available to vegetation (e.g., Roderick et al. 2014; Greve et al. 2014; Byrne and O'Gorman 2015). As such, when assessing changes to the viticulture indices under future climate, growing-season precipitation–evapotranspiration (GSP-EVT) was also included as an additional index. This index is calculated by subtracting total evapotranspiration over the growing season from GSP and gives an indication of how much water is available for use by the grapevine. It was not possible to include this index in the evaluation section as no observational data for evapotranspiration were available. We note that the dryness index of Tonietto and Carbonneau (2004) is essentially GSP-EVT but includes a soil water reserve term, which represents the amount of soil water available to the roots. Although soil moisture outputs are available from WRF over four soil layers, there is a lack of information about the rooting depths of different varieties of grapevines as well as a lack of soil moisture observations at different depths. Hence, we only show differences in

TABLE 1. Table showing the time period used for the calculation, class limits, and sources for HI and CI.

Index	Months	Class limits	Source
HI [Eq. (1)]	1 Oct–31 Mar	Very cool = ≤1500 Cool = 1500–1800 Temperate = 1800–2100 Warm temperate = 2100–2400 Warm = 2400–3000 Very warm = >3000	Huglin (1978)
CI [Eq. (2)]	1–31 Mar	Very cool nights = ≤12 Cool nights = 12–14 Temperate nights = 14–18 Warm nights = >18	Tonietto and Carbonneau (2004)

GSP-EVT and do not include soil water available to roots.

e. Data analysis

1) MODEL EVALUATION

To enable intercomparison, the AWAP observational dataset of temperature and precipitation were interpolated from the original regular grid (5-km resolution) to the rotated latitude–longitude projection of the WRF domain (5-km resolution) using simple inverse-distance weighting. The rotated latitude–longitude projection is one of the many projection options available in WRF, and more details can be found in Wang et al. (2015). This particular projection was used as it is the recommended projection following CORDEX guidelines (available at https://www.cordex.org). The first part of the analysis involved evaluating WRF-ERA's simulation of each index against observations. Spatial model agreement was examined with bias contour plots (WRF minus observations) for the whole wine region. Subsequently, spatial and temporal agreement with observations was assessed by using the metrics of pattern correlation [corr; Eq. (4)], which describes spatial agreement, centered root-mean-square differences [RMSDs; Eq. (5)], which is a measure of the average magnitude of model error, and variance ratios [VRs; Eq. (8)], which describe the difference between the observed and simulated average annual variance. These metrics were summarized in a Taylor diagram, which is a commonly used diagram for examining climate model simulations (Taylor 2001). A regional analysis of biases was also undertaken by computing regionally averaged absolute (WRF minus observations) and percentage [(WRF minus observations/observations) × 100] biases for each of the wine regions. Last, the ability of WRF-ERA to reproduce the interannual variability of the indices was evaluated through a comparison of the observed and simulated annual anomalies from 1981 to 2010 for each of the indices, averaged over all of the wine regions.

The second stage of the analysis involved evaluating the GCM-forced simulations against observations. For this, the analysis that was carried out was identical to that for WRF-ERA except that annual anomalies were not computed as an RCM driven with a GCM can only be expected to reproduce the mean climate over at least 10–30 years rather than the climate for one particular year. Also, this analysis covered the period from 1981 to 1999 to enable comparisons between WRF-ERA and the WRF simulations driven by the GCMs under current climate.

The formulas for calculating the corr, the centered RMSD, the annual variance for the observations σ_o^2 and simulation σ_s^2, and the annual VR are given below, where s is the simulated field, o is the observed field, and the overall mean of a field is indicated by an overbar:

$$\text{corr} = \frac{\frac{1}{N}\sum_{n=1}^{N}(s_n - \bar{s})(o_n - \bar{o})}{\sigma_s \sigma_o}, \tag{4}$$

$$\text{RMSD} = \frac{1}{N}\sum_{n=1}^{N}[(s_n - \bar{s})(o_n - \bar{o})]^2, \tag{5}$$

$$\sigma_s^2 = \frac{1}{N}\sum_{n=1}^{N}(s_n - \bar{s})^2, \tag{6}$$

$$\sigma_o^2 = \frac{1}{N}\sum_{n=1}^{N}(o_n - \bar{o})^2, \quad \text{and} \tag{7}$$

$$\text{VR} = \frac{\sigma_o^2}{\sigma_s^2}. \tag{8}$$

TABLE 2. The length-of-day coefficient K for HI (Huglin 1978).

Lat	K
≤40°00′	1.00
40°01′–42°00′	1.02
42°01′–44°00′	1.03
44°01′–46°00′	1.04
46°01′–48°00′	1.05
48°01′–50°00′	1.06

2) FUTURE CLIMATE PROJECTIONS

Climate projections were analyzed from each GCM-driven simulation and their ensemble mean through an analysis of future minus present climate contour plots for each climate index. This is known as the delta change approach and is a simple and frequently used method for overcoming some of the bias issues associated with climate modeling (Liang et al. 2008; Ruml et al. 2012). This approach is based on the assumption that a model's bias is constant in time so that by subtracting the present climate from the future climate, the bias is effectively removed, and the amount of climate change to be expected can be quantified.

The difference between future climate and present climate was tested for statistical significance using the Zwiers and von Storch *t* test at a 95% confidence interval for each index (Zwiers and von Storch 1995). This *t* test is a statistical tool that was specifically developed for analyzing small samples ($\leq$30) of climate data. It is suitable for this application as it takes into account the serial correlation of the data. The assumptions of the test are that the two samples are Gaussian and serially correlated with the same variance and lag-1 correlation (Zwiers and von Storch 1995). The Zwiers and von Storch *t* test has been used widely in climate research for testing differences between two climate means (Deser et al. 2004; Räisänen et al. 2004; Jungclaus et al. 2010; Reda 2015; Chiodo et al. 2016).

3. Results

a. *Evaluation of WRF-ERA against observations (1981–2010)*

In this section, WRF simulations that have been driven with ERA-Interim are compared with the AWAP observations to quantify WRF's downscaling capabilities for SWWA in relation to the climatic indices relevant to viticulture. The indices are evaluated for the period 1981–2010.

Figure 3 shows the observed and simulated indices and the corresponding model biases averaged over the period 1981–2010. There was a clear north–south temperature gradient for the observed HI (Fig. 3a). HI ranged from 2900 units in the north of the region to 1800 units on the southeast coast (Fig. 3a). According to the Tonietto and Carbonneau (2004) classification (Table 1), this spans the "warm" to "temperate" temperature regimes. The north–south decreasing temperature gradient was well represented by WRF-ERA, and biases were predominantly warm for HI (Fig. 3a). The observed CI was warmest along the west and southeast coastlines (14°–17°C) and coldest in the center of the state's wine region (12°–14°C; Fig. 3b), ranging from "cool" to "temperate" nights as classified by Tonietto and Carbonneau (2004; Table 1). Again, WRF-ERA was able to capture this general pattern of CI well, and biases were ±1°C across most of the region (Fig. 3b). Some areas, however, had a bias of up to 2°C, particularly in the center, where CI was observed to be coldest. A warm bias of up to 2°C was also noted in a corner of the southwestern tip.

The observed GSP increased from north to south and showed an initial increase from west to east, coinciding with the location of the Darling Scarp, before decreasing again (Fig. 3c). Wine regions along the south coast were found to experience up to 400 mm per growing season and as little as 180 mm per growing season in the north and east. WRF-ERA was able to represent a north–south increasing rainfall gradient for GSP but with less definition than what was observed. The observed west–east gradient was only slightly evident in the simulation, and WRF-ERA did not capture the extent of the increase of rainfall along the scarp (Fig. 3c). Bias was predominantly dry with the exception of some wet bias on the eastern part of the region, and bias was largest along the coast and the Darling Scarp.

Figure 4 shows a Taylor diagram for the three climate indices. These plots graphically summarize how well the simulated indices match the observed indices in terms of their corr [Eq. (4)], RMSD [Eq. (5)], and average annual VR [Eq. (8); Taylor 2001]. The arc on the Taylor diagram shows the corr, while the *x* and *y* axes indicate the VR. The dashed line labeled REF highlights where the VR is equal to 1, and the concentric semicircles that increase around the point on the *x* axis labeled REF represent the RMSD, with each contour representing 0.5 RMSD. Good model agreement with observations is represented by the index point being found close to the *x* axis and near the REF line.

Pattern correlation was high (corr $>$ 0.85) for all of the indices, particularly for HI (corr $>$ 0.95). GSP had the lowest pattern correlation (corr = 0.87). RMSDs were $<$1 for the temperature indices and only slightly greater than 1 for GSP. The VR for HI was slightly greater than 1, indicating that the average annual variance was less than observed, and just below 1 for CI and GSP, indicating the contrary.

Regionally averaged biases indicate that model agreement was highest for CI (Fig. 5). Simulated CI did not differ by more than ±1°C from the observations for any of the regions, and biases were all $<$10%. Biases were predominantly positive, but there was a slight underestimation of CI in Margaret River (Fig. 1). Regionally averaged biases for HI were all positive (Fig. 5a) and larger than those for CI. However, regional biases were still mostly $<$10%. The exceptions were the

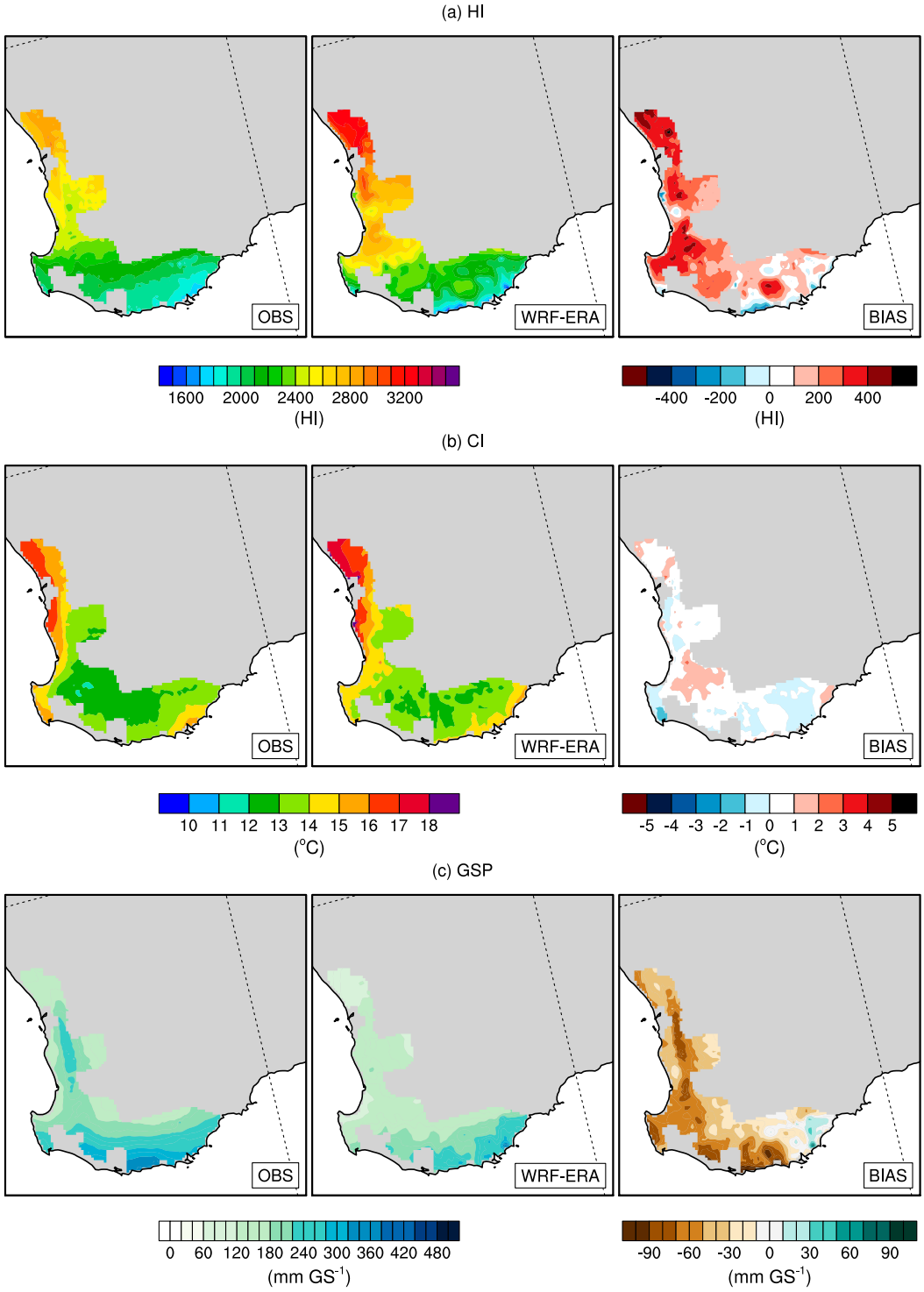

FIG. 3. OBS, WRF-ERA simulation, and bias (WRF − OBS) for (a) HI, (b) CI, and (c) GSP (for the October–April growing season; in this and subsequent figures, per growing season is indicated as GS^{-1}) averaged from 1981 to 2010.

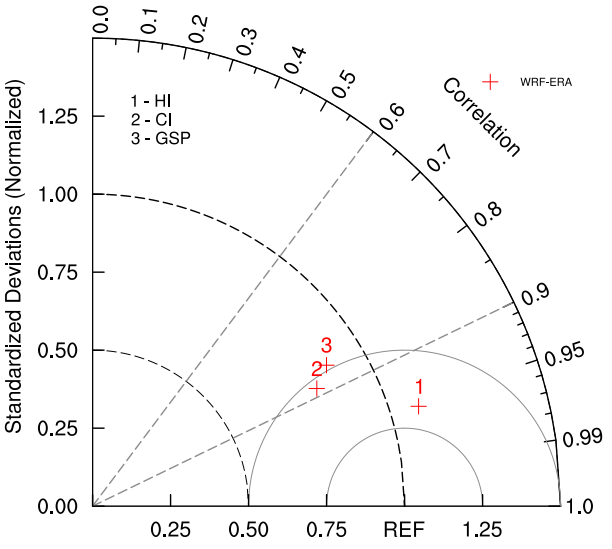

FIG. 4. Taylor plot showing spatial and temporal agreement of WRF-ERA with observations for HI, CI, and GSP (for the October–April growing season) from 1981 to 2010 (RMSD contour interval = 0.5). Labels 1, 2, and 3 refer to HI, CI, and GSP, respectively.

Perth Hills (12.0%), the Swan District (13.1%), and Geographe (11.9%). Average regional biases were consistently negative for GSP and substantially higher than what was found for the temperature indices (Fig. 5c). All biases > 20% with the exception of the Great Southern (13.0%), and Margaret River had the greatest percentage bias at just over 30%.

Figure 6 shows that the observed annual anomalies did not indicate any observable trend in the indices over the given time period (no statistical test was applied). Anomalies for HI were generally well represented by WRF-ERA (Fig. 6a). However, model agreement for interannual variability was poor across some years. Notable discrepancies were for the years 1991, 2001, and 2003. The observed interannual variability for CI was also well captured by WRF-ERA, with the simulation consistently showing a close match with observations across the given time period. An exception was the year 2007, which was a cooler than average year but was simulated as slightly warmer than average (Fig. 6b). For GSP, the observed anomalies had a poorer representation by WRF-ERA, with several years showing marked discrepancies between observations and the simulation. Notable examples were the years 1985, 1989, 1990, 1994, 2001, 2003, and 2005 (Fig. 6c).

b. *Evaluation of WRF-CCS, WRF-CSI, and WRF-ECH against observations (1981–99)*

Following on from the evaluation of WRF-ERA's simulation against observations, and with an understanding of the biases associated with WRF, the next section explores WRF's ability to reproduce the climate indices relevant to viticulture when using boundary conditions from three GCMs for the period 1981–99. WRF-ERA was included in this evaluation as a reference point to measure model skill.

Figures 7–9 show the observed and simulated temperature indices with corresponding biases for WRF-ERA, WRF-CCS, WRF-CSI, and WRF-ECH averaged from 1981 to 1999. All of the GCM-forced simulations were able to represent the north–south temperature gradient across WA's wine regions for HI. Similarly, CI's pattern of warmer temperatures along the coast and cooler values in the center was also simulated by all models. The north–south gradient for GSP was also well captured by the simulations, but precipitation around the Darling Scarp was poorly represented. All of the simulations had predominantly dry biases, most notably along the coastline and the Darling Scarp. WRF-CCS and WRF-ECH demonstrated a slight wet bias in the southeast (Fig. 9).

Pattern correlation was high for all simulations of HI (>0.95) and reasonable for CI (0.85 < corr <0.90; Fig. 10). There was little difference in corr values between simulations, and HI generally had the greatest spatial agreement for all simulations. For the temperature indices, the VRs for WRF-CCS and WRF-CSI were >1, indicating simulated annual variance was, on average, greater than observed. This discrepancy was largest for WRF-CSI's simulation of HI, as evidenced by the high VR and RMSD. WRF-ECH, on the other hand, had VRs all <1 for the temperature indices, showing that this simulation had higher annual variance. For GSP, WRF-CCS had the greatest spatial agreement with observations (corr = 0.83); however, it had a markedly high VR (>3) and RMSD (>5). WRF-CSI had the lowest pattern correlation with observations (corr = 0.62). Both WRF-CSI and WRF-ECH overestimated the average annual variance with VRs < 1.

The distribution, sign, and magnitude of the regional biases identified in WRF-CCS's simulation of the temperature indices were closely aligned with what was found for WRF-ERA's simulations (Figs. 11a,b and 12a,b). For CI, biases were lowest for WRF-CCS relative to the other GCM-forced simulations. For the temperature indices, WRF-CSI had a notably warmer tendency and showed the least skill. For HI and CI, WRF-CSI had average regional warm biases that exceeded 30% and 60% in some regions, respectively (Figs. 11 and 12). For HI, WRF-ECH had regional biases that were smaller than all other simulations, including WRF-ERA (mostly <10%; Fig. 11).

Average regional biases show that GSP was predominantly underestimated by all simulations and across all regions with the exception of a slight overestimation

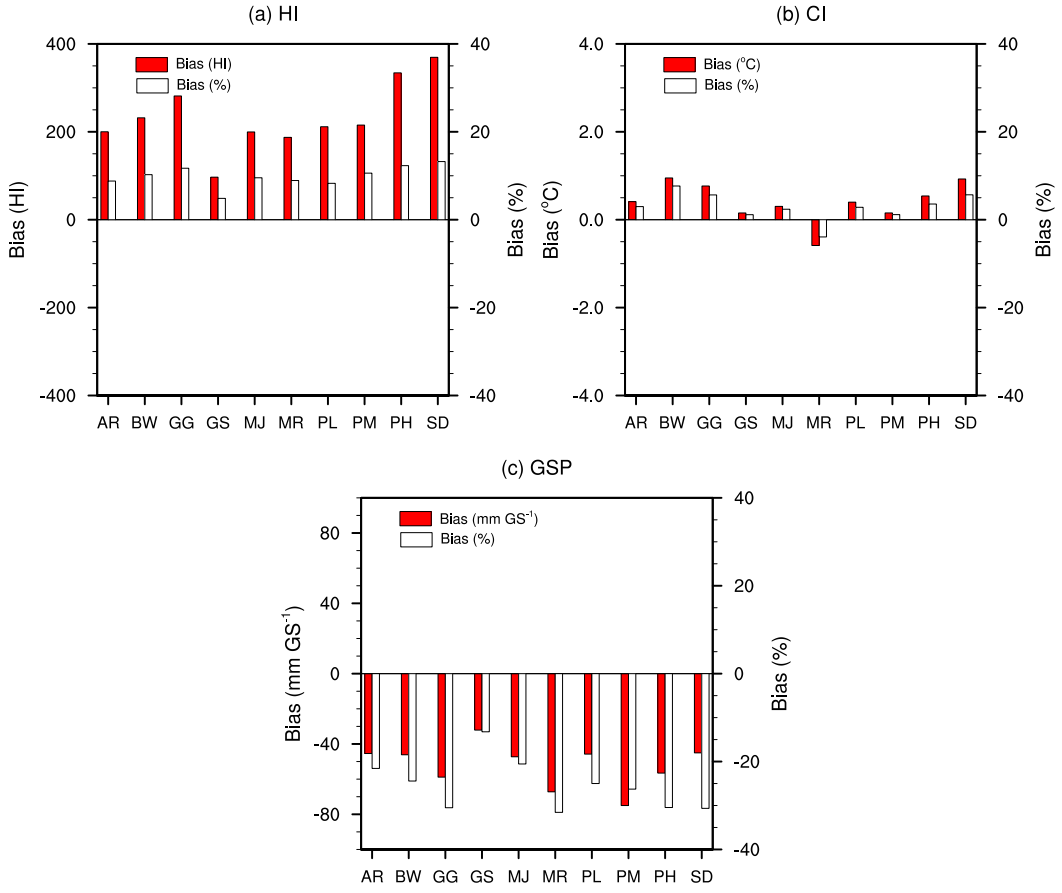

FIG. 5. Absolute (red) and percentage (white) bias for WRF-ERA over the period 1981–2010 averaged across all regions (AR), Blackwood Valley (BV), Geographe (GG), Great Southern (GS; here also used as a region label), Manjimup (MJ), Peel (PL), Pemberton (PM), Perth Hills (PH), and Swan District (SD) for (a) HI, (b) CI, and (c) GSP (for the October–April growing season).

by WRF-ECH in the Great Southern and Manjimup (Fig. 13). WRF-ECH showed the greatest accuracy in reproducing GSP when compared with the other simulations, with substantially lower biases across all regions. This simulation had particularly good agreement with observations for Blackwood Valley, Manjimup, the Great Southern, and the Swan District (bias $< 10\%$). WRF-ERA, WRF-CCS, and WRF-CSI all had a similar pattern of regional biases for GSP, but biases were generally larger for WRF-CCS. For WRF-CCS and WRF-CSI, biases for GSP exceeded 30% for all regions with the exception of WRF-CSI in the Great Southern, where the bias was just under 20% (Fig. 13).

c. *Climate projections (2030–59 minus 1970–99)*

Having quantified the errors associated with WRF and the GCM-forced simulations, future changes to the viticulture indices are now quantified by applying the delta change method of future (2030–59) minus current (1970–99) climate for the three GCM-forced simulations and their ensemble mean.

The simulations projected increases in both temperature indices across all of WA's wine regions (Fig. 14). All of these changes were statistically significant with the exception of an inland part in the north of the region for WRF-ECH's simulation of CI. For the temperature indices, WRF-CSI projected the greatest degree of warming. Furthermore, projected warming had a north–south decreasing trend. There was less model agreement with regard to future changes in GSP (Fig. 14c). WRF-CCS projected large decreases in GSP, WRF-CSI projected little change but some drying in the north and southeast, and WRF-ECH projected an increase in precipitation in the north and southeast and some decrease in the southwest. The ensemble mean projected an overall decline in GSP. However, the projected changes were not statistically significant with the exception of a small area in the north for WRF-CSI. As with GSP, projections for GSP-EVT varied between ensemble members. WRF-CCS

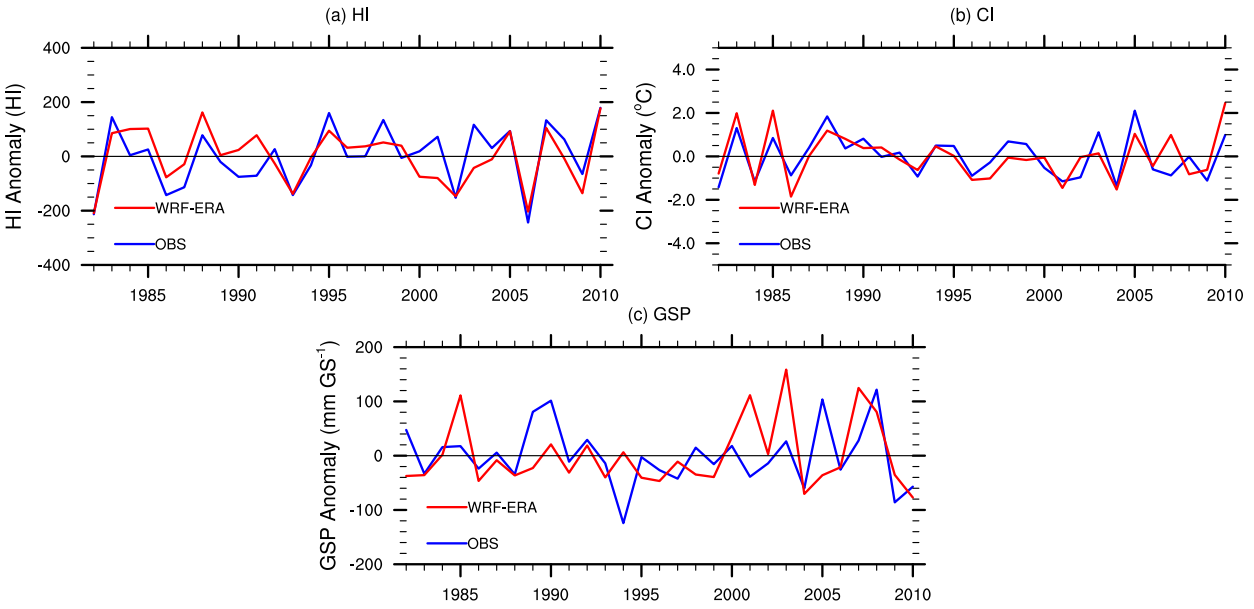

FIG. 6. Time series [1981–2010 (series begins in 1982, which represents the 1981/82 growing season)] comparing OBS and simulated (WRF-ERA) annual anomalies averaged over the whole wine region for (a) HI, (b) CI, and (c) GSP (for the October–April growing season).

projected increases to the index in the northeast and southeast and decreases in the southwest. Statistically significant change was only identified in the southeast. WRF-CSI projected little change, and WRF-ECH suggested GSP-EVT will increase across most of the region, particularly in the north and northeast, with only a small area projected to experience statistically significant change. The ensemble mean showed minimal change across most of the region, with some significant increases in the north, northeast, and southeast.

For all simulations, the regionally averaged projected change indicated that HI will increase by >220 units in all regions, with the northern regions projected to increase by up to 400 units (Fig. 15a). The southern regions were projected to have lower increases in HI. There was little difference in the magnitude of projected warming between the simulations for HI. For CI, all regions were projected to experience warming of at least 1°C by all simulations, with WRF-CSI projecting larger increases of approximately 2°C across most of the regions. The ensemble mean projected a minimum of 1.4°C regionwide. For GSP, differences between simulations were particularly marked, most notably in the large reduction in GSP projected by WRF-CCS (Fig. 15c). For the ensemble mean, changes were projected to be largest for Pemberton (−95 mm per growing season) and smallest for the Swan District (−40 mm per growing season). Projected regional changes in GSP-EVT varied markedly between regions and simulations. Averaged across all regions, GSP-EVT was projected to increase. Generally, less change was projected for the regions in the south and southwest (<15 mm per growing season), and larger changes were projected for the regions in the north (up to 45 mm per growing season). WRF-ECH projected notably larger increases in the northern regions relative to the other ensemble members.

4. Discussion and conclusions

a. WRF regional climate simulations using ERA-Interim boundary conditions

This study has shown that when WRF is driven with ERA-Interim data, the RCM provides a satisfactory representation of the indices that are relevant to viticulture, particularly for the temperature indices. Average regional percentage biases were largely <10% for the temperature indices (Fig. 5), and WRF was shown to have a dominant warmer tendency. Andrys et al. (2015) highlighted a prominent cold bias for maximum temperatures in these WRF simulations of SWWA climate. This deficiency in WRF has also been highlighted in other regional climate studies for SWWA (Kala et al. 2015), United States (Zhang et al. 2009), and Europe (Dasari et al. 2014; Heikkilä et al. 2011; Katragkou et al. 2015; Soares et al. 2012). However, the viticulture-related indices evaluated in the present study include HI, which incorporates an average of maximum and minimum temperatures, and CI, which is the average minimum temperature in March. Therefore, WRF's

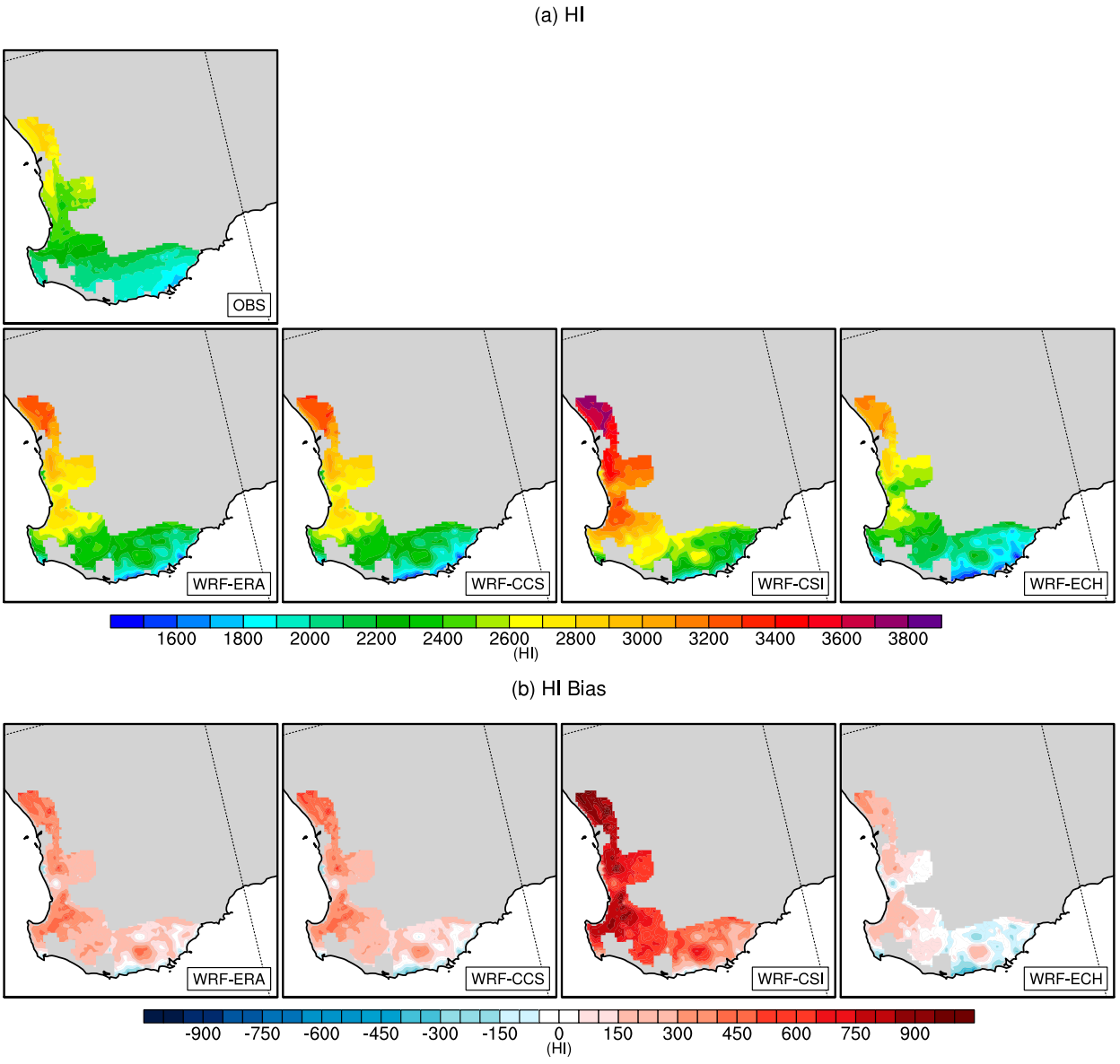

FIG. 7. (a) OBS and simulated HI for WRF-ERA, WRF-CCS, WRF-CSI, and WRF-ECH and (b) biases (WRF − OBS) for all simulations averaged over the period 1981–99.

specific bias characteristics are less identifiable because of averaging resulting in masked biases. This highlights a shortfall of the study in that, by using averages for model evaluation, the distinct model bias characteristics can be hidden through bias compensation, which has the potential to incorrectly indicate model skill. This is also an issue that has been highlighted in other model evaluation studies (García-Díez et al. 2013; Katragkou et al. 2015; Perkins et al. 2007). Notwithstanding, the skill shown for the other performance measures of corr, RMSD, and VR (Fig. 4), which are all independent of model biases, provides a reliable endorsement for the use of WRF to investigate changes to the indices relevant to viticulture in WA's wine regions.

For the temperature indices, CI was simulated with the greatest accuracy, with average regional percentage biases largely <5%. There were slightly larger biases associated with the simulation of HI, which may be related to the method of calculation. Because HI is a heat summation index whereby temperatures are summed over the growing season, bias is accumulated over this time frame. The bias calculated for CI, however, is an average of the biases associated with the simulation of minimum temperatures during March. Minimum temperatures are generally influenced by topography

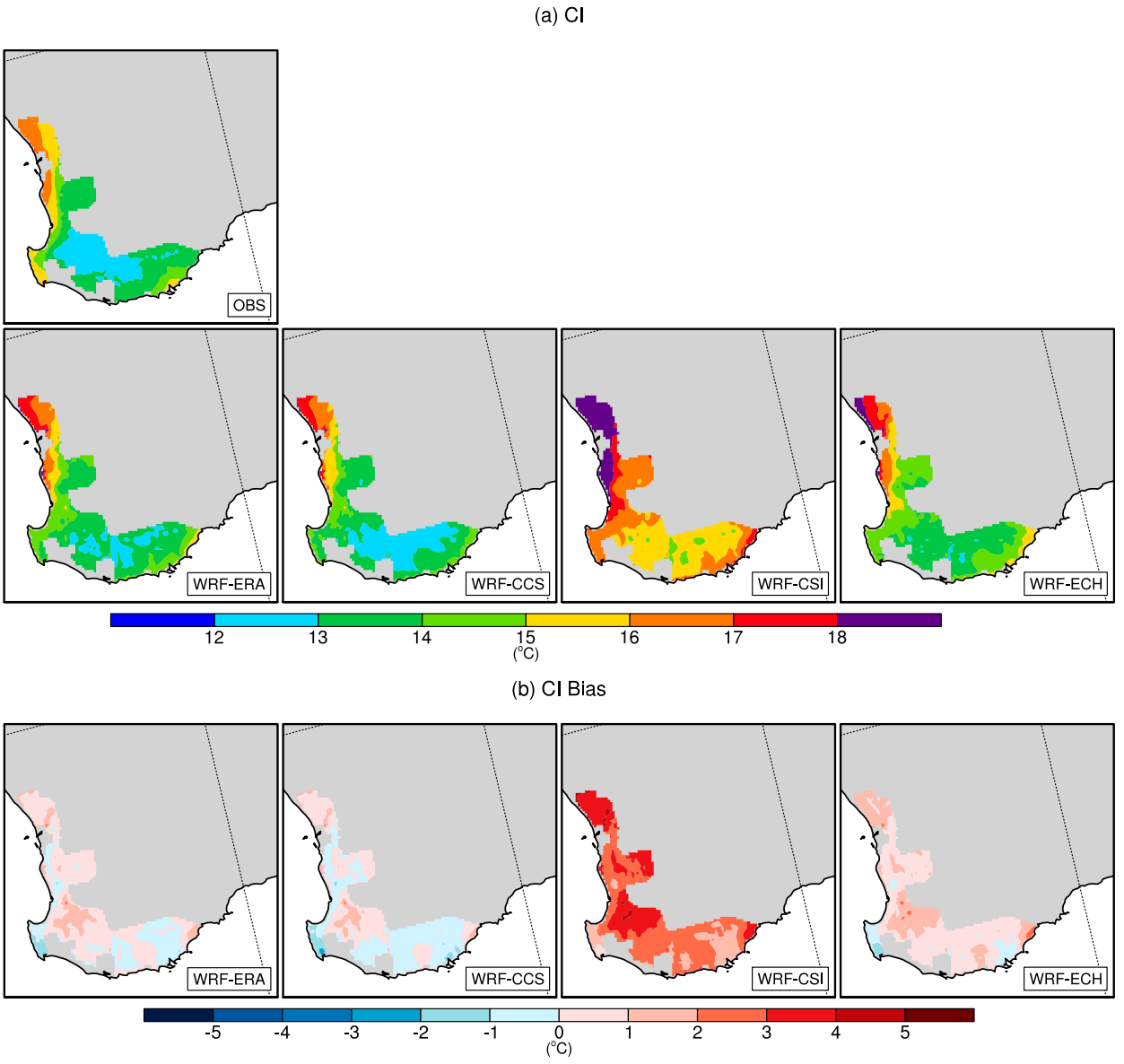

FIG. 8. As in Fig. 7, but for CI.

to a greater extent than maximum temperatures because of cold air drainage at night (e.g., Chung et al. 2006; Hubbart et al. 2007; Bigg et al. 2014), and errors associated with the simulation of minimum temperatures are therefore usually related to the resolution of the climate model limiting the accurate representation of finer-scale features (Perkins et al. 2007). Pattern correlation for CI was slightly lower in comparison with HI but still within an acceptable range (corr = 0.88; Fig. 4). A finding of lower pattern correlation values for minimum temperatures is consistent with other comparable regional climate evaluations (Andrys et al. 2015; Soares et al. 2012; Zhang et al. 2009). The predominantly warm biases that were identified in WRF-ERA's simulation of CI are consistent with the findings of Andrys et al. (2015) for WRF's simulation of minimum temperatures in spring. A warm bias for WRF's simulation of minimum temperatures was also identified by Kala et al. (2015) in SWWA.

WRF was found to have larger errors when simulating precipitation than it did for the temperature-related indices, which is a common finding in climate modeling research (Chotamonsak et al. 2011; Salathe et al. 2010). The magnitude and distribution of rainfall are strongly influenced by local features such as topography. SWWA is characterized by relatively low relief; therefore,

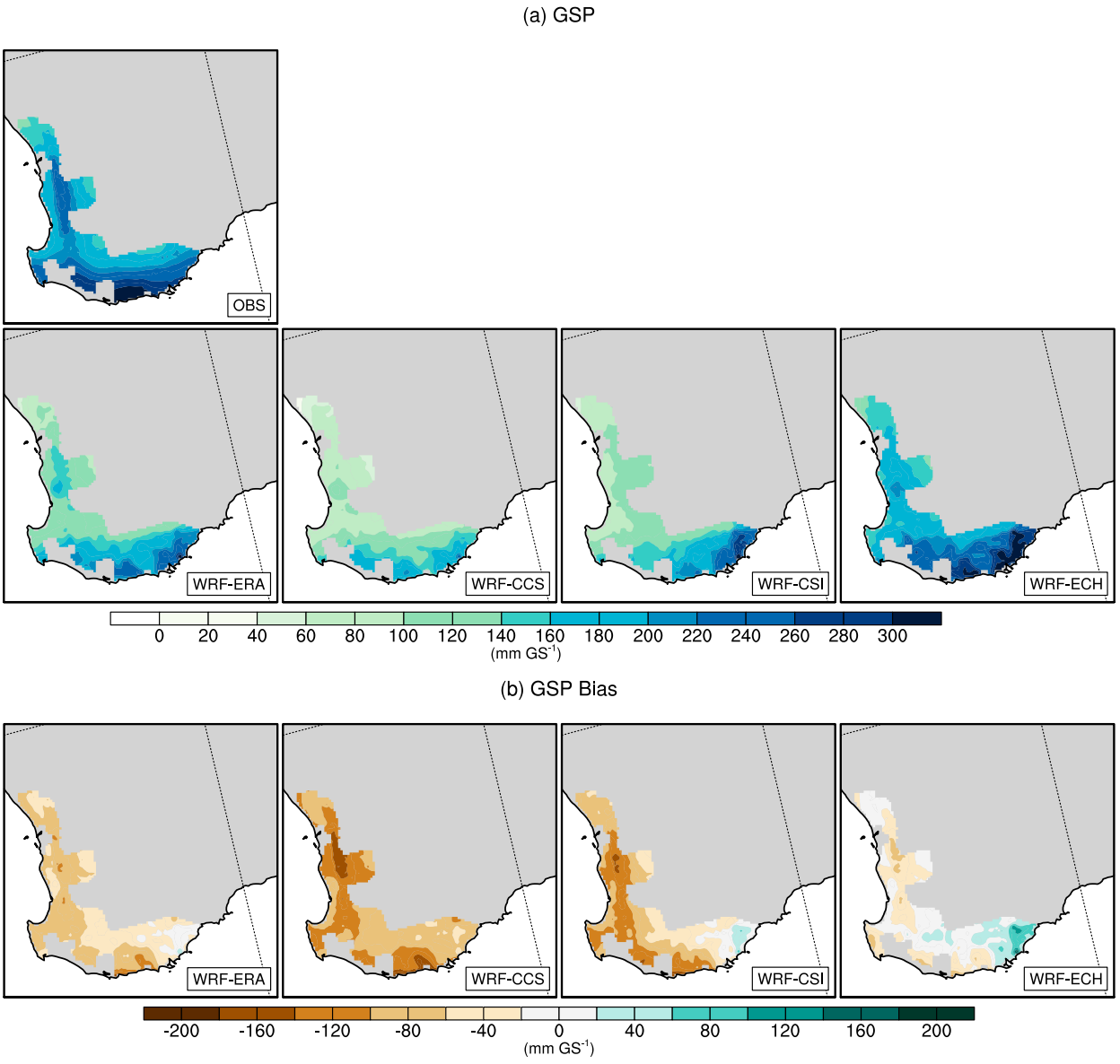

FIG. 9. As in Fig. 7, but for GSP.

topography is not a primary influence on its climate. However, the Darling Scarp does generate an increase in rainfall in its vicinity, as noted in the observed GSP (Fig. 3c). Because of the resolution of the climate simulations analyzed (5 km), this precipitation pattern has not been fully captured by WRF-ERA, as evidenced by the negative bias found in this area. In a study by Pitts and Lyons (1990), it was shown that a resolution of 0.5 km was needed to accurately reproduce the wind-generated turbulence of the scarp and hence its potential influence on local precipitation patterns. Furthermore, rainfall during the growing season in SWWA is generally low as the majority of the region's rainfall occurs during winter. The main driver of the climate in this region is the position of the subtropical high pressure belt. During spring and summer, it is located to the south of SWWA, with the associated cold fronts located farther south of the continent, resulting in hot, dry conditions for the region as anticyclonic conditions dominate. During autumn, the high pressure belt migrates northward and is positioned at SWWA's northern boundary during winter, allowing for the regular passage of cold fronts that bring the majority of the annual rainfall to SWWA (Gentilli 1972). Rainfall that occurs during the growing season (i.e., late spring, summer, and early autumn) is generally strongly influenced

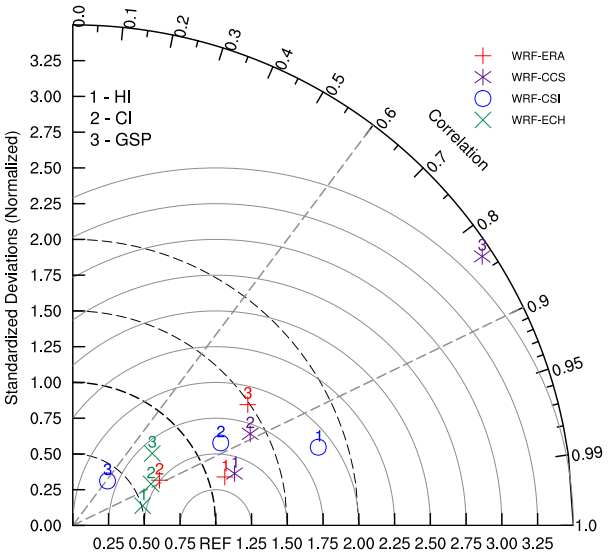

FIG. 10. Taylor plot comparing spatial and temporal agreement of WRF-ERA, WRF-CCS, WRF-CSI, and WRF-ECH with observations for HI, CI, and GSP (for the October–April growing season) for the period 1981–99 (RMSD contour interval = 0.5). Labels 1, 2, and 3 refer to HI, CI, and GSP, respectively.

by surface heating and associated convection, a process that is known to be difficult for climate models to simulate accurately (Harding et al. 2013; Heikkilä et al. 2011).

Biases across the region were predominantly negative for GSP, with just a slight wet bias in the southeast (Fig. 3c). When averaged for the regions, this was completely masked by the dominant dry bias (Fig. 5c). This is in contrast to findings from other studies that have used WRF as an RCM to simulate precipitation and found the overestimation of precipitation to be more characteristic of WRF (Argüeso et al. 2012; Caldwell et al. 2009; Heikkilä et al. 2011; Katragkou et al. 2015). However, all of these studies ran WRF at a coarser resolution of 10–36 km and in regions with comparatively complex topography. There is a known tendency of RCMs to overestimate precipitation on the windward side of topographical features, known as the windward/lee effect, when their resolution is not fine enough to effectively resolve convection (Wulfmeyer et al. 2008). The finer resolution of 5 km used in this study could be a reason why such biases were not found, but these differences could also be due to different physics options used by these other studies using WRF. A significant dry bias was identified along the southwest coastline. This issue was also highlighted by Andrys et al. (2015), who showed that the dry bias along the coast could be explained by the western domain boundary being too close to the coastline. This was shown by carrying out an additional simulation during 2007 (when the bias was highest) but extending the western boundary of the domain by an additional 10 grid points (50 km) into the Indian Ocean, thus providing additional distance between the domain boundary and the coastline. Andrys et al. (2015) showed that this reduced the dry bias to a large extent but not completely. Similar edge effects have been reported elsewhere (Seth and Giorgi 1998; Lowrey and Yang 2008). There were no observable trends in GSP over the period 1981–2010. This is consistent with previous studies on climatic trends in the region, which have found a clear decreasing trend in rainfall in the region during winter (June–August) since the mid-1970s, but not during other seasons (Allan and Haylock 1993; Smith et al. 2000; Hope et al. 2006).

b. *WRF regional climate simulations using GCM boundary conditions*

The WRF-ERA simulation, being driven with a reanalysis product, provides a useful reference for comparison with WRF simulations driven with GCMs. The close alignment between WRF-ERA and WRF-CCS in terms of the magnitude, sign, and regional distribution of biases associated with the temperature indices (Figs. 7 and 8) indicates that the quality of the driving data in this simulation is superior to that of the other GCMs for temperature-related indices. This is in support of the findings of Andrys et al. (2016), where WRF-CCS was found to consistently score higher on performance-based measures when simulating temperature in SWWA relative to the other GCM-forced simulations.

WRF-CSI had a prominent warmer tendency that was not present in the other simulations and, in terms of biases, showed the least skill in simulating the temperature indices. The warm bias that has been highlighted in WRF-CSI is consistent with the findings of Andrys et al. (2016), where a positive bias was identified in WRF-CSI's simulations of the climate in SWWA for both minimum and maximum temperatures but particularly for minima. The distinct contrast in WRF-CSI's simulation of the temperature indices to that of the other GCM-forced simulations indicates that the warm bias has been inherited by the input driving data.

The sign of the biases exhibited by WRF-ECH's simulation of the temperature indices also largely matched the sign of those found for WRF-ERA. However, the magnitude was lower for HI and comparable for CI (Figs. 7 and 8). WRF-ECH performed better than WRF-CSI, a finding that differs from that of Andrys et al. (2016), where the two members were generally found to be comparable in terms of performance, both having equally significant errors but of different

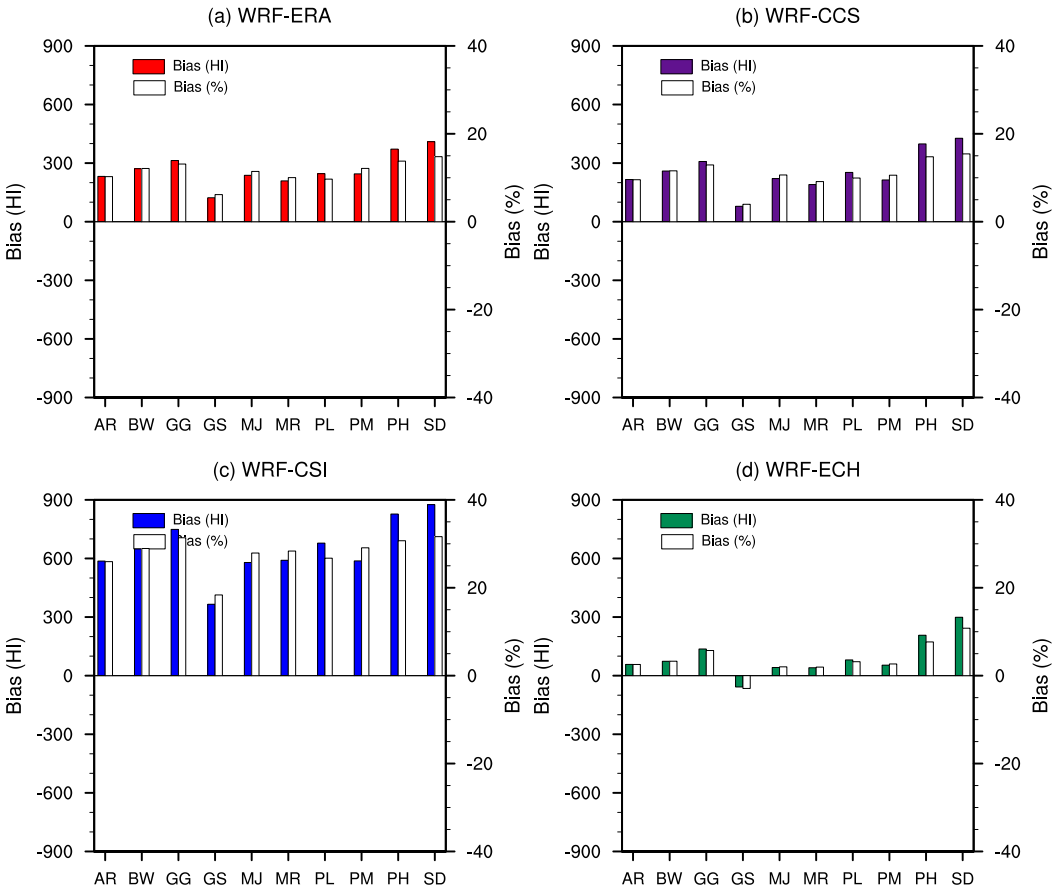

FIG. 11. The HI absolute (red) and percentage (white) bias (WRF − OBS) averaged across AR, BV, GG, GS (here used as a region label), MJ, PL, PM, PH, and SD for (a) WRF-ERA, (b) WRF-CCS, (c) WRF-CSI, and (d) WRF-ECH over the period 1981–99.

characteristics. The improved performance of WRF-ECH to that of WRF-CSI in simulating the indices relevant to viticulture can be related to the calculation of the indices, which ultimately reflects the error characteristics in different ways. For example, a systematic cold bias of up to 5°C was identified in WRF-ECH by Andrys et al. (2016), which has effectively counteracted the warm bias inherent in the simulation of HI shared by all ensemble members. WRF-ECH was found by Andrys et al. (2016) to perform well when simulating minimum temperatures, which is further supported by the low biases associated with its simulation of CI. Conversely, the simulation of minimum temperatures was where WRF-CSI was found to be poorest, hence its notable overestimation of CI. Despite these biases, pattern correlation values for the temperature indices were high ($0.85 < \text{corr} < 0.97$) and similar for all simulations (Fig. 10). This indicates that WRF is able to accurately reproduce the spatial pattern of temperature in these regions despite the large-scale biases introduced by the driving data.

The biases suggest that WRF-ECH reproduced the observed GSP more accurately than the other simulations, even improving upon WRF-ERA (Fig. 13). However, pattern correlation was second to lowest (corr = 0.74), next to WRF-CSI, for GSP, indicating the spatial distribution of rainfall was poor for WRF-ECH (Fig. 10). Andrys et al. (2016) examined seasonal rainfall biases in SWWA produced by the same GCM-driven simulations that are analyzed here. WRF-ECH was found to have a more persistent wet bias than the other simulations while also exhibiting some dry bias, particularly in spring and along the coast in winter. Therefore, by looking at total rainfall over the growing season, the biases in the WRF-ECH simulation are effectively masked. The biases for this simulation are therefore low but for the ''wrong'' reasons rather than as a result of model skill, hence an example of bias compensation. Further work on the frequency, intensity, and timing of precipitation simulations throughout the growing season is therefore required to better understand these biases.

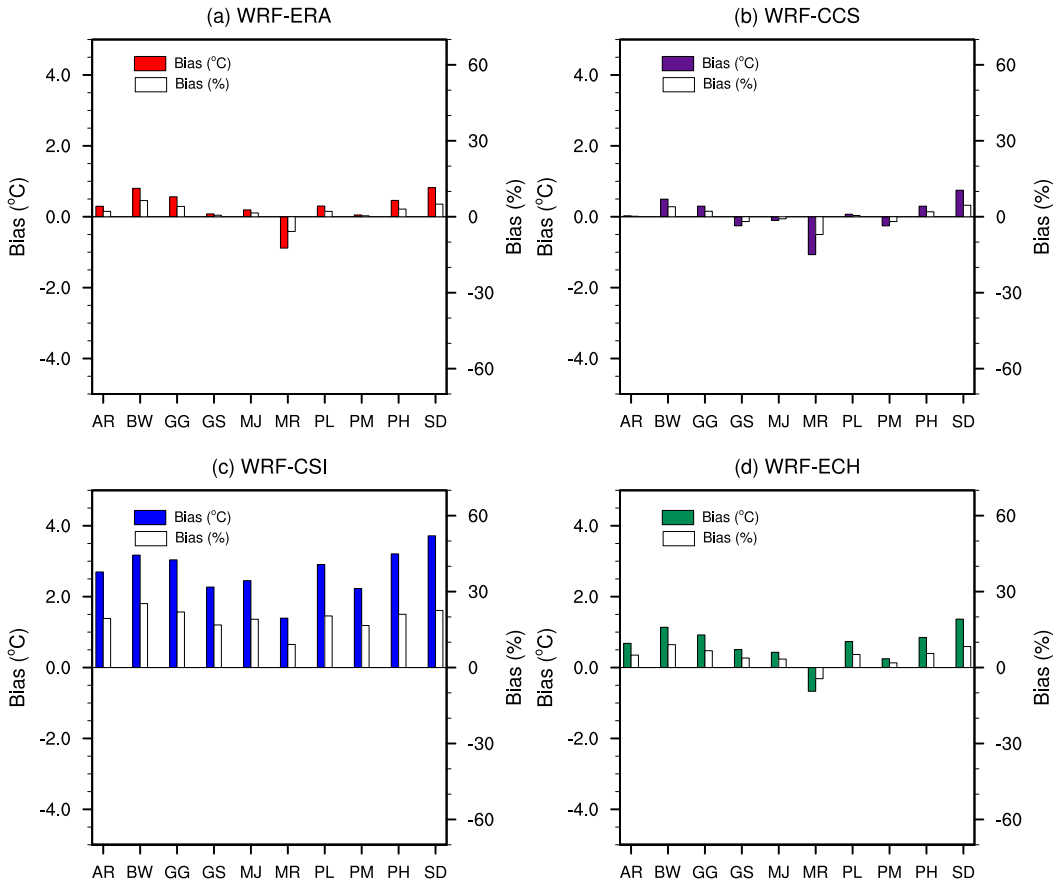

FIG. 12. As in Fig. 11, but for CI.

Model performance with respect to the simulation of GSP was inconsistent for all ensemble members. For example, although spatial correlation for GSP was best for WRF-CCS, biases, RMSD, and VRs were notably high, with biases exceeding 60% in the northern wine regions (Fig. 13b). This large bias for WRF-CCS is likely to be related to the fact that winter precipitation is not included in GSP. Winter was the only season where WRF-CCS was found by Andrys et al. (2016) to exhibit a wet bias. Hence, by not including this season, the dry bias found for the other seasons is more notable. The inconsistency demonstrated by the three ensemble members in simulating GSP diminishes confidence in the use of these simulations to quantify future changes to this index in the wine regions of WA. Any use of the GSP results should therefore take into consideration the high uncertainty with respect to future changes in precipitation.

In summary, it can be concluded that WRF-CCS offers a superior representation of the temperature-related indices that are important to viticulture in WA's wine regions when compared with WRF-CSI and WRF-ECH. For GSP, however, all simulations had significant shortfalls when reproducing this index for WA's wine regions, with no ensemble member showing any distinct advantage over the others.

c. *WRF regional climate projections for viticulture in Western Australia*

Based on the findings of this research, where climate projections were based on the assumptions of the A2 emission scenario, all of WA's wine regions are expected to experience statistically significant increases in HI under future climate (Fig. 14). Significant increases in CI were also projected for all regions and all simulations with the exception of WRF-ECH, where part of the region was projected to not experience any significant change. WRF-CSI was generally found to result in a higher warming scenario when compared with the other simulations, which is a distinction that was also made by Webb et al. (2008) and Barnuud (2012) when comparing climate projections from CMIP3 GCMs for WA's wine regions.

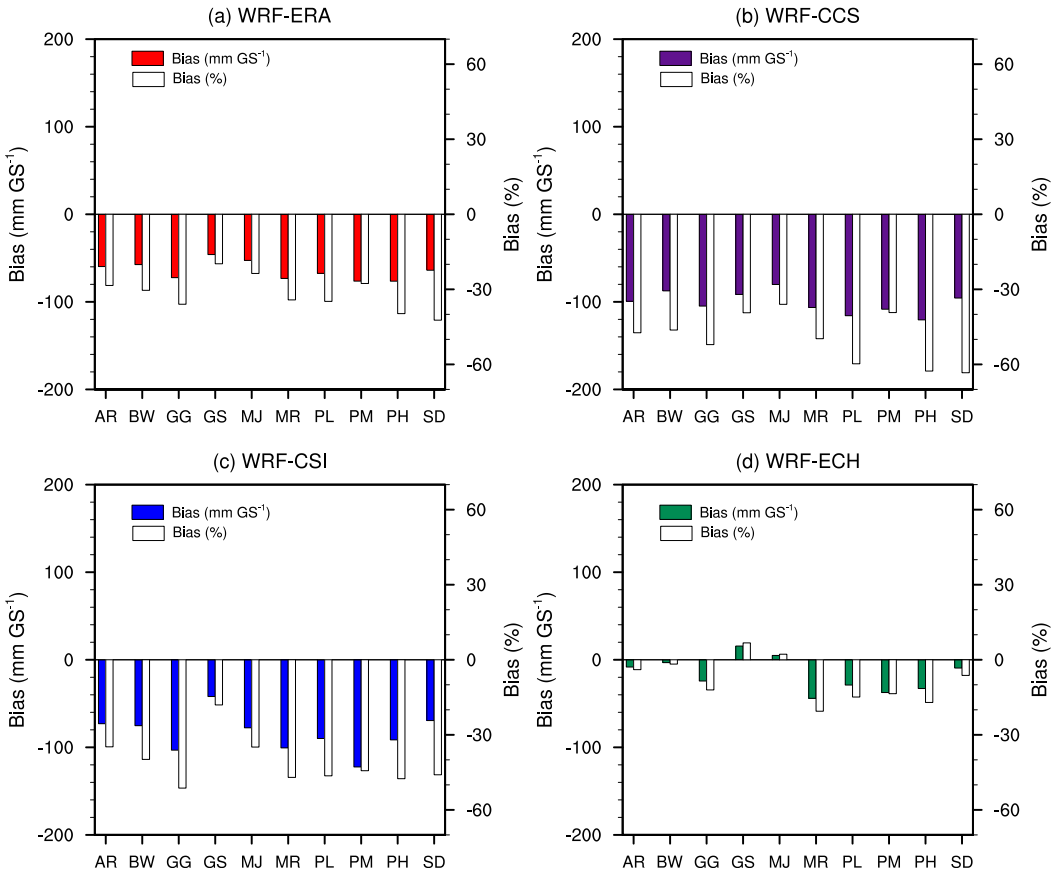

FIG. 13. As in Fig. 11, but for GSP.

Although there were some differences in the magnitude of projected warming, all simulations agreed on the direction of change, which increases confidence in the projections.

Regional differences in the projected warming of HI were not marked, although the Swan District and the Perth Hills were projected to have a slightly larger increase than the other regions (Fig. 15a). These regions at the north of WA's viticulture area are already experiencing warm growing conditions. The projected increases in HI would push them into the ''very warm'' classification (Table 1), potentially challenging the regions' capacity to produce premium quality wines. The most southern regions and central west regions, which currently fall into the ''temperate'' and ''warm temperate'' categories for HI, would be reclassified as ''warm temperate'' and ''warm,'' respectively. Such changes could lead to future growing conditions being more favorable for alternative varieties to those that are currently grown. Several European studies have also highlighted how increases in HI will lead to some viticulture regions no longer being viable for premium wine production (Seguin 2005; Stock et al. 2005) and a shift in varieties for other regions (Fraga et al. 2013; Lorenzo et al. 2013; Moral et al. 2016).

Other studies that have evaluated climate projections for viticulture-related climate indices in WA's wine regions have also highlighted the vulnerability of WA's wine industry, particularly for the northern regions. For example, Hall and Jones (2009) found that WA's northern wine regions would potentially experience growing conditions in the future that would deem them no longer viable for premium wine production. These included the Perth Hills and Swan District by 2030, Peel by 2050, and Geographe by 2070. This was also supported by the findings of Barnuud (2012), who also classified north Blackwood as no longer viable for premium wine production by 2070. Research that has evaluated the potential impacts of climate change on the quality of wine produced in WA has also highlighted the wine region's vulnerability, particularly for the hotter northern regions. For example, Webb et al. (2008) carried out a regionally specific evaluation of climate change impacts for Australia's viticulture industry for 2030 and 2050 under scenarios of low, medium, and high

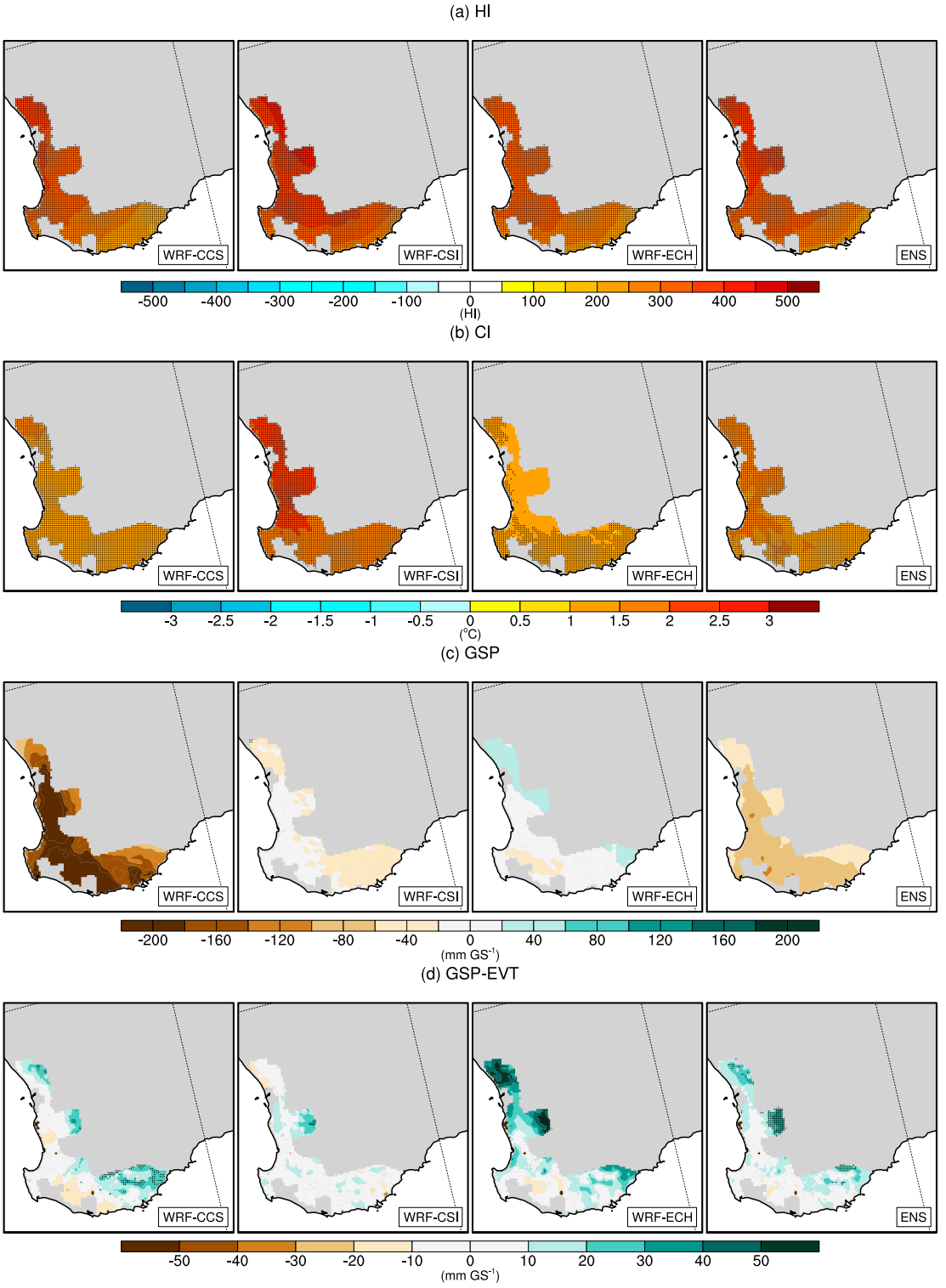

FIG. 14. Differences between future (2030–59) and historical (1970–99) simulations from WRF-CCS, WRF-CSI, WRF-ECH, and their ensemble mean for (a) HI, (b) CI, (c) GSP (for the October–April growing season), and (d) GSP-EVT. Stippling shows areas where there is a statistically significant difference at a 95% confidence interval.

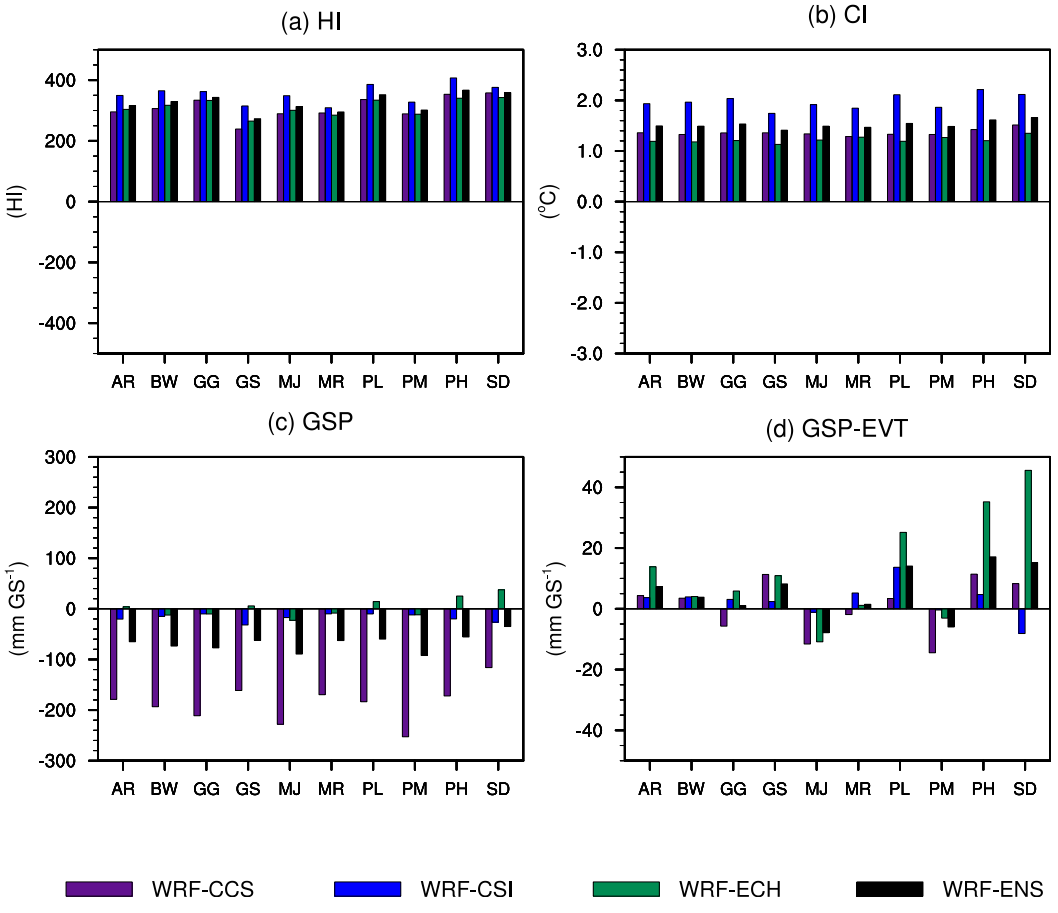

FIG. 15. Projected change (2030–59 minus 1970–99) from WRF-CCS, WRF-CSI, WRF-ECH, and their ensemble mean averaged across AR, BV, GG, GS (here also used as a region label), MJ, PL, PM, PH, and SD for (a) HI, (b) CI, (c) GSP (for the October–April growing season), and (d) GSP-EVT.

warming. The cost to premium wine grape quality was quantified, and the Swan District was projected to experience up to 100% cost to quality by 2050, whereas the Great Southern and Margaret River, in the cooler south, were projected to entail lower costs to quality of up to 15% and 20%, respectively. Hence, the results presented here, based on high-resolution climatic data, provide a strong reinforcement to findings from previous research that have indicated WA's wine regions will face challenges under future climate.

Current CI classifications of WA's wine regions range from "temperate nights" in the Swan District and the Perth Hills to "cool nights" in the cooler central regions (Fig. 3b; Table 1). The ensemble mean climate projection suggested that all regions would experience a warming of at least 1.4°C for CI, with slightly more warming projected for the Swan District and the Perth Hills (Fig. 15b). This could result in the northern regions being reclassified as "warm nights" under future climate. Higher nocturnal temperatures during the ripening period are associated with a loss of aroma in the resulting wine as well as a lightening of color in red wines (Tonietto and Carbonneau 2004). It is acknowledged that in WA, it is possible for wine grapes to be harvested prior to the month of March, depending on the variety and season conditions. Therefore, the CI, as it is calculated here, would not be applicable in such cases. Further research that modified the CI to apply to the specific ripening period of certain varieties would provide greater value when investigating how changes to this index may impact viticulture in WA. Notwithstanding, the findings clearly point to a warmer climate, the implications of which for WA's wine regions could be a change of identity for the wine industry. For example, while the state's wine regions are currently most well known for specific varieties of premium quality, future climate could lead to a shift in varieties, such as from cooler climate white varieties to red varieties more suited to warmer conditions.

There was less agreement between models with regard to changes to GSP and GSP-EVT in WA's wine

regions. While projections for GSP indicated largely drier conditions, projections for GSP-EVT suggested an increase in water availability under future climate, with notable variability between ensemble members for both indices. There is therefore greater uncertainty as to how these indices will change under future climate. This ambiguity related to future precipitation projections is a common issue in climate change research because climate models are not able to simulate rainfall with the same accuracy as temperature (Alexander and Arblaster 2009).

This research explored a range of plausible climate projections for the climate indices relevant to viticulture in WA by evaluating WRF simulations that were driven with three different GCMs. However, because of data availability, the project was limited to one RCM and one SRES emissions scenario; thus, the full range of uncertainty related to the future climate of WA's wine region was not taken into account. Furthermore, the climate data that were available for evaluation were produced from WRF simulations driven by CMIP3 GCMs. However, CMIP5 GCMs (Taylor et al. 2012) currently represent the state of the art for GCMs. Therefore, it is acknowledged that there are now improved datasets available for carrying out climate change evaluations than what has been used in this research. Nonetheless, CMIP3 GCMs are still very useful and still widely used as boundary conditions for regional climate studies (e.g., Fita et al. 2017; Evans et al. 2017; Olson et al. 2016).

Because there were significant biases identified in the WRF simulations, it was not possible to evaluate the absolute values projected for the indices and then relate those to the established climatic thresholds for different varieties. A warm bias of 2°C, for example, could inaccurately indicate that a temperature threshold had been exceeded. To reduce these biases, future research will make use of ERA-Interim as a surrogate truth to correct biases from the GCMs prior to use as boundary conditions in WRF. This method has recently been successfully implemented to reduce biases from WRF regional climate simulations driven with GCMs (e.g., Xu and Yang 2012; Yu and Wang 2014; Bruyère et al. 2014). Another method that will also be investigated will be to reduce biases from the current temperature and precipitation simulations by bias correcting the latter against the AWAP gridded observations, following the methodology of Argüeso et al. (2013), who bias corrected WRF temperature and precipitation simulations over southeast Australia. Applying these bias correction methods would minimize the identified biases, thus facilitating an evaluation of thresholds. This would enable an assessment of current varietal suitability based on established thresholds and of how this may change under future climate. Considering that the productive lifespan of the grapevine is expected to be >50 years, a current understanding of what varieties will be most suited to future climate can be of high value.

Acknowledgments. Julia Andrys is supported by an Australian Postgraduate Award and a GRDC Top Up Scholarship. Computational modeling was supported by the Pawsey Supercomputing Centre with funding from the Australian Government and the Government of Western Australia. The project was funded under the National Computational Merit Allocation Scheme and the Pawsey Partner Allocation Scheme. The comments of three anonymous reviewers helped to improve the manuscript. All of this support is gratefully acknowledged.

REFERENCES

Alexander, L. V., and J. M. Arblaster, 2009: Assessing trends in observed and modelled climate extremes over Australia in relation to future projections. *Int. J. Climatol.*, **29**, 417–435, doi:10.1002/joc.1730.

Allan, R. J., and M. R. Haylock, 1993: Circulation features associated with the winter rainfall decrease in southwestern Australia. *J. Climate*, **6**, 1356–1367, doi:10.1175/1520-0442(1993)006<1356:CFAWTW>2.0.CO;2.

Andrys, J., T. J. Lyons, and J. Kala, 2015: Multidecadal evaluation of WRF downscaling capabilities over Western Australia in simulating rainfall and temperature extremes. *J. Appl. Meteor. Climatol.*, **54**, 370–394, doi:10.1175/JAMC-D-14-0212.1.

——, ——, and ——, 2016: Evaluation of a WRF ensemble using GCM boundary conditions to quantify mean and extreme climate for the southwest of Western Australia (1970–1999). *Int. J. Climatol.*, **36**, 4406–4424, doi:10.1002/joc.4641.

——, J. Kala, and T. J. Lyons, 2017: Regional climate projections of mean and extreme climate for the southwest of Western Australia (1970–1999 compared to 2030–2059). *Climate Dyn.*, **48**, 1723–1747, doi:10.1007/s00382-016-3169-5.

Argüeso, D., J. M. Hidalgo-Muñoz, S. R. Gámiz-Fortis, M. J. Esteban-Parra, and Y. Castro-Díez, 2012: Evaluation of WRF mean and extreme precipitation over Spain: Present climate (1970–99). *J. Climate*, **25**, 4883–4897, doi:10.1175/JCLI-D-11-00276.1.

——, J. P. Evans, and L. Fita, 2013: Precipitation bias correction of very high resolution regional climate models. *Hydrol. Earth Syst. Sci.*, **17**, 4379–4388, doi:10.5194/hess-17-4379-2013.

Barnuud, N. N., 2012: Determining climate change impacts on viticulture in Western Australia. Ph.D. dissertation, Curtin University, 206 pp. [Available online at http://espace.library.curtin.edu.au:80/R?func=dbin-jump-full&local_base=gen01-era02&object_id=186490.]

——, A. Zerihun, M. Gibberd, and B. Bates, 2014a: Berry composition and climate: Responses and empirical models. *Int. J. Biometeor.*, **58**, 1207–1223, doi:10.1007/s00484-013-0715-2.

——, ——, F. Mpelasoka, M. Gibberd, and B. Bates, 2014b: Responses of grape berry anthocyanin and titratable acidity to the projected climate change across the Western Australian wine regions. *Int. J. Biometeor.*, **58**, 1279–1293, doi:10.1007/s00484-013-0724-1.

Bates, B. C., P. Hope, B. Ryan, I. Smith, and S. Charles, 2008: Key findings from the Indian Ocean Climate Initiative and their

impact on policy development in Australia. *Climatic Change*, **89**, 339–354, doi:10.1007/s10584-007-9390-9.

Bigg, G. R., S. M. Wise, E. Hanna, D. Mansell, R. G. Bryant, and A. Howard, 2014: Synoptic climatology of cold air drainage in the Derwent Valley, Peak District, UK. *Meteor. Appl.*, **21**, 161–170, doi:10.1002/met.1317.

Bonnardot, V., and S. Cautenet, 2009: Mesoscale atmospheric modeling using a high horizontal grid resolution over a complex coastal terrain and a wine region of South Africa. *J. Appl. Meteor. Climatol.*, **48**, 330–348, doi:10.1175/2008JAMC1710.1.

——, ——, G. Cautenet, M. Déqué, and H. Quénol, 2014: Modélisation méso-échelle du changement climatique: Le cas des vignobles français. *Changement climatique et terroirs viticoles*, Lavoisier, 317–332. [Available online at https://hal.archives-ouvertes.fr/hal-01011461.]

Bonnefoy, C., 2013: Observation et modélisation spatiale de la température dans les terroirs viticoles du val de loire dans le contexte du changement climatique. Ph.D. thesis, Université de Rennes, 322 pp.

Bruyère, C. L., J. M. Done, G. J. Holland, and S. Fredrick, 2014: Bias corrections of global models for regional climate simulations of high-impact weather. *Climate Dyn.*, **43**, 1847–1856, doi:10.1007/s00382-013-2011-6.

Byrne, M. P., and P. A. O'Gorman, 2015: The response of precipitation minus evapotranspiration to climate warming: Why the wet-get-wetter, dry-get-drier scaling does not hold over land. *J. Climate*, **28**, 8078–8092, doi:10.1175/JCLI-D-15-0369.1.

Cabré, M. F., H. Quénol, and M. Nuñez, 2016: Regional climate change scenarios applied to viticultural zoning in Mendoza, Argentina. *Int. J. Biometeor.*, **60**, 1325–1340, doi:10.1007/s00484-015-1126-3.

Caldwell, P., H.-N. S. Chin, D. C. Bader, and G. Bala, 2009: Evaluation of a WRF dynamical downscaling simulation over California. *Climatic Change*, **95**, 499–521, doi:10.1007/s10584-009-9583-5.

Charles, S., and Coauthors, 2010: Climate analyses for south-west Western Australia. CSIRO Tech. Rep., 92 pp., doi:10.4225/08/584d9590d046b.

Chen, F., and J. Dudhia, 2001: Coupling an advanced land surface–hydrology model with the Penn State–NCAR MM5 modeling system. Part I: Model implementation and sensitivity. *Mon. Wea. Rev.*, **129**, 569–585, doi:10.1175/1520-0493(2001)129<0569:CAALSH>2.0.CO;2.

Chiodo, G., R. García-Herrera, N. Calvo, J. M. Vaquero, J. A. Añel, D. Barriopedro, and K. Matthes, 2016: The impact of a future solar minimum on climate change projections in the northern hemisphere. *Environ. Res. Lett.*, **11**, 034015, doi:10.1088/1748-9326/11/3/034015.

Chotamonsak, C., E. P. Salath, J. Kreasuwan, S. Chantara, and K. Siriwitayakorn, 2011: Projected climate change over southeast Asia simulated using a WRF regional climate model. *Atmos. Sci. Lett.*, **12**, 213–219, doi:10.1002/asl.313.

Christensen, J. H., T. R. Carter, M. Rummukainen, and G. Amanatidis, 2007: Evaluating the performance and utility of regional climate models: The PRUDENCE project. *Climatic Change*, **81**, 1–6, doi:10.1007/s10584-006-9211-6.

Chung, U., H. Seo, K. Hwang, B. Hwang, J. Choi, J. Lee, and J. Yun, 2006: Minimum temperature mapping over complex terrain by estimating cold air accumulation potential. *Agric. For. Meteor.*, **137**, 15–24, doi:10.1016/j.agrformet.2005.12.011.

Clarke, R., 1989: Sea-breezes and waves: The Kalgoorlie seabreeze and the Goondiwindi breeze. *Aust. Meteor. Mag.*, **37**, 99–107.

Collins, W. D., and Coauthors, 2006: The Community Climate System Model version 3 (CCSM3). *J. Climate*, **19**, 2122–2143, doi:10.1175/JCLI3761.1.

Dasari, H. P., R. Salgado, J. Perdigao, and V. S. Challa, 2014: A regional climate simulation study using WRF-ARW model over Europe and evaluation for extreme temperature weather events. *Int. J. Atmos. Sci.*, **2014**, 704079, doi:10.1155/2014/704079.

Dee, D. P., and Coauthors, 2011: The ERA-Interim reanalysis: Configuration and performance of the data assimilation system. *Quart. J. Roy. Meteor. Soc.*, **137**, 553–597, doi:10.1002/qj.828.

Deser, C., A. S. Phillips, and J. W. Hurrell, 2004: Pacific interdecadal climate variability: Linkages between the tropics and the North Pacific during boreal winter since 1900. *J. Climate*, **17**, 3109–3124, doi:10.1175/1520-0442(2004)017<3109:PICVLB>2.0.CO;2.

Duchêne, E., and C. Schneider, 2005: Grapevine and climatic changes: A glance at the situation in Alsace. *Agron. Sustainable Dev.*, **25**, 93–99, doi:10.1051/agro:2004057.

Dudhia, J., 1989: Numerical study of convection observed during the Winter Monsoon Experiment using a mesoscale two-dimensional model. *J. Atmos. Sci.*, **46**, 3077–3107, doi:10.1175/1520-0469(1989)046<3077:NSOCOD>2.0.CO;2.

En-Tao, Y., W. Hui-Jun, and S. Jian-Qi, 2010: A quick report on a dynamical downscaling simulation over China using the nested model. *Atmos. Oceanic Sci. Lett.*, **3**, 325–329, doi:10.1080/16742834.2010.11446886.

Evans, J. P., and M. F. McCabe, 2010: Regional climate simulation over Australia's Murray-Darling basin: A multitemporal assessment. *J. Geophys. Res.*, **115**, D14114, doi:10.1029/2010JD013816.

——, D. Argueso, R. Olson, and A. Di Luca, 2017: Bias-corrected regional climate projections of extreme rainfall in south-east Australia. *Theor. Appl. Climatol.*, doi:10.1007/s00704-016-1949-9, in press.

Fita, L., J. P. Evans, D. Argüeso, A. King, and Y. Liu, 2017: Evaluation of the regional climate response in Australia to large-scale climate modes in the historical NARCliM simulations. *Climate Dyn.*, doi:10.1007/s00382-016-3484-x, in press.

Fraga, H., A. C. Malheiro, J. Moutinho-Pereira, and J. A. Santos, 2012: An overview of climate change impacts on European viticulture. *Food Energy Secur.*, **1**, 94–110, doi:10.1002/fes3.14.

——, ——, ——, and ——, 2013: Future scenarios for viticultural zoning in Europe: Ensemble projections and uncertainties. *Int. J. Biometeor.*, **57**, 909–925, doi:10.1007/s00484-012-0617-8.

——, ——, ——, G. V. Jones, F. Alves, J. G. Pinto, and J. A. Santos, 2014: Very high resolution bioclimatic zoning of Portuguese wine regions: Present and future scenarios. *Reg. Environ. Change*, **14**, 295–306, doi:10.1007/s10113-013-0490-y.

——, I. García de Cortázar Atauri, A. C. Malheiro, and J. A. Santos, 2016: Modelling climate change impacts on viticultural yield, phenology and stress conditions in Europe. *Global Change Biol.*, **22**, 3774–3788, doi:10.1111/gcb.13382.

García-Díez, M., J. Fernández, L. Fita, and C. Yagüe, 2013: Seasonal dependence of WRF Model biases and sensitivity to PBL schemes over Europe. *Quart. J. Roy. Meteor. Soc.*, **139**, 501–514, doi:10.1002/qj.1976.

Gentilli, J., 1972: *Australian Climate Patterns.* Thomas Nelson, 285 pp.

Giorgi, F., C. Jones, and G. R. Asrar, 2009: Addressing climate information needs at the regional level: The CORDEX framework. *WMO Bull.*, **58**, 175–183.

Gordon, H. B., and Coauthors, 2002: The CSIRO Mk3 climate system model. CSIRO Atmospheric Research Tech. Rep. 60, 130 pp. [Available online at https://publications.csiro.au/rpr/download?pid=procite:ff94db7e-ad41-40bf-b6be-2ab1ad07805c&dsid=DS1.]

Grell, G. A., S. Emeis, W. R. Stockwell, T. Schoenemeyer, R. Forkel, J. Michalakes, R. Knoche, and W. Seidl, 2000: Application of a multiscale, coupled MM5/chemistry model to the complex terrain of the VOTALP valley campaign. *Atmos. Environ.*, **34**, 1435–1453, doi:10.1016/S1352-2310(99)00402-1.

Greve, P., B. Orlowsky, B. Mueller, J. Sheffield, M. Reichstein, and S. I. Seneviratne, 2014: Global assessment of trends in wetting and drying over land. *Nat. Geosci.*, **7**, 716–721, doi:10.1038/ngeo2247.

Gula, J., and W. R. Peltier, 2012: Dynamical downscaling over the Great Lakes Basin of North America using the WRF regional climate model: The impact of the Great Lakes system on regional greenhouse warming. *J. Climate*, **25**, 7723–7742, doi:10.1175/JCLI-D-11-00388.1.

Hall, A., and G. V. Jones, 2009: Effect of potential atmospheric warming on temperature-based indices describing Australian winegrape growing conditions. *Aust. J. Grape Wine Res.*, **15**, 97–119, doi:10.1111/j.1755-0238.2008.00035.x.

Harding, K. J., P. K. Snyder, and S. Liess, 2013: Use of dynamical downscaling to improve the simulation of central U.S. warm season precipitation in CMIP5 models. *J. Geophys. Res. Atmos.*, **118**, 12 522–12 536, doi:10.1002/2013JD019994.

Hasumi, H., and S. Emori, 2004: K-1 coupled GCM (MIROC) description. Center for Climate System Research Tech. Rep. 1, 34 pp. [Available online at http://ccsr.aori.u-tokyo.ac.jp/~hasumi/miroc_description.pdf.]

Heikkilä, U., A. Sandvik, and A. Sorteberg, 2011: Dynamical downscaling of ERA-40 in complex terrain using the WRF regional climate model. *Climate Dyn.*, **37**, 1551–1564, doi:10.1007/s00382-010-0928-6.

Hewitson, B., J. Daron, R. Crane, M. Zermoglio, and C. Jack, 2014: Interrogating empirical-statistical downscaling. *Climatic Change*, **122**, 539–554, doi:10.1007/s10584-013-1021-z.

Hirsch, A. L., A. J. Pitman, and J. Kala, 2014a: The role of land cover change in modulating the soil moisture-temperature land-atmosphere coupling strength over Australia. *Geophys. Res. Lett.*, **41**, 5883–5890, doi:10.1002/2014GL061179.

——, ——, S. I. Seneviratne, J. P. Evans, and V. Haverd, 2014b: Summertime maximum and minimum temperature coupling asymmetry over Australia determined using WRF. *Geophys. Res. Lett.*, **41**, 1546–1552, doi:10.1002/2013GL059055.

Hong, S.-Y., and J.-O. J. Lim, 2006: The WRF single-moment 6-class microphysics scheme (WSM6). *J. Korean Meteor. Soc.*, **42**, 129–151.

——, J. Dudhia, and S.-H. Chen, 2004: A revised approach to ice microphysical processes for the bulk parameterization of clouds and precipitation. *Mon. Wea. Rev.*, **132**, 103–120, doi:10.1175/1520-0493(2004)132<0103:ARATIM>2.0.CO;2.

Hope, P. K., 2006: Projected future changes in synoptic systems influencing southwest Western Australia. *Climate Dyn.*, **26**, 765–780, doi:10.1007/s00382-006-0116-x.

——, W. Drosdowsky, and N. Nicholls, 2006: Shifts in the synoptic systems influencing southwest Western Australia. *Climate Dyn.*, **26**, 751–764, doi:10.1007/s00382-006-0115-y.

Hubbart, J. A., K. L. Kavanagh, R. Pangle, T. Link, and A. Schotzko, 2007: Cold air drainage and modeled nocturnal leaf water potential in complex forested terrain. *Tree Physiol.*, **27**, 631–639, doi:10.1093/treephys/27.4.631.

Huglin, P., 1978: Nouveau mode d'évaluation des possibilités héliothermiques d'un milieu viticole. *C. R. Acad. Agric. Fr.*, **64**, 1117–1126.

Jones, D. A., W. Wang, R. Fawcett, and I. Grant, 2007: Climate data for the Australian Water Availability Project: Final milestone report. Australian Bureau of Meteorology Rep., 36 pp.

Jones, G. V., 2007: Climate change: Observations, projections, and general implications for viticulture and wine production. Whitman College Economics Dept. Working Paper 7, 15 pp.

——, and G. B. Goodrich, 2008: Influence of climate variability on wine regions in the western USA and on wine quality in the Napa Valley. *Climate Res.*, **35**, 241–254, doi:10.3354/cr00708.

Jungclaus, J., and Coauthors, 2010: Climate and carbon-cycle variability over the last millennium. *Climate Past*, **6**, 723–737, doi:10.5194/cp-6-723-2010.

Kain, J. S., 2004: The Kain–Fritsch convective parameterization: An update. *J. Appl. Meteor.*, **43**, 170–181, doi:10.1175/1520-0450(2004)043<0170:TKCPAU>2.0.CO;2.

Kala, J., J. Andrys, T. J. Lyons, I. J. Foster, and B. J. Evans, 2015: Sensitivity of WRF to driving data and physics options on a seasonal time-scale for the southwest of Western Australia. *Climate Dyn.*, **44**, 633–659, doi:10.1007/s00382-014-2160-2.

Kalnay, E., and Coauthors, 1996: The NCEP/NCAR 40-Year Reanalysis Project. *Bull. Amer. Meteor. Soc.*, **77**, 437–471, doi:10.1175/1520-0477(1996)077<0437:TNYRP>2.0.CO;2.

Katragkou, E., and Coauthors, 2015: Regional climate hindcast simulations within EURO-CORDEX: Evaluation of a WRF multi-physics ensemble. *Geosci. Model Dev.*, **8**, 603–618, doi:10.5194/gmd-8-603-2015.

Keeling, C. D., S. C. Piper, R. B. Bacastow, M. Wahlen, T. P. Whorf, M. Heimann, and H. A. Meijer, 2001: Exchanges of atmospheric CO_2 and $^{13}CO_2$ with the terrestrial biosphere and oceans from 1978 to 2000. I. Global aspects. Scripps Institution of Oceanography Tech. Rep. 01–06, 28 pp. [Available online at http://scrippsco2.ucsd.edu/assets/publications/keeling_sio_ref_series_exchanges_of_co2_ref_no_01-06_2001.pdf.]

King, A. D., L. V. Alexander, and M. G. Donat, 2013: The efficacy of using gridded data to examine extreme rainfall characteristics: A case study for Australia. *Int. J. Climatol.*, **33**, 2376–2387, doi:10.1002/joc.3588.

Liang, X.-Z., K. E. Kunkel, G. A. Meehl, R. G. Jones, and J. X. L. Wang, 2008: Regional climate models downscaling analysis of general circulation models present climate biases propagation into future change projections. *Geophys. Res. Lett.*, **35**, L17S19, doi:10.1029/2008GL033666.

Lorenzo, M. N., J. J. Taboada, J. F. Lorenzo, and A. M. Ramos, 2013: Influence of climate on grape production and wine quality in the Rías Baixas, north-western Spain. *Reg. Environ. Change*, **13**, 887–896, doi:10.1007/s10113-012-0387-1.

Lowrey, M. R. K., and Z.-L. Yang, 2008: Assessing the capability of a regional-scale weather model to simulate extreme precipitation patterns and flooding in central Texas. *Wea. Forecasting*, **23**, 1102–1126, doi:10.1175/2008WAF2006082.1.

Mlawer, E. J., S. J. Taubman, P. D. Brown, M. J. Iacono, and S. A. Clough, 1997: Radiative transfer for inhomogeneous atmospheres: RRTM, a validated correlated-*k* model for the longwave. *J. Geophys. Res.*, **102**, 16 663–16 682, doi:10.1029/97JD00237.

Moral, F. J., F. J. Rebollo, L. L. Paniagua, A. García, and E. M. de Salazar, 2016: Application of climatic indices to analyse viticultural suitability in Extremadura, south-western Spain. *Theor. Appl. Climatol.*, **123**, 277–289, doi:10.1007/s00704-014-1363-0.

Moriondo, M., G. V. Jones, B. Bois, C. Dibari, R. Ferrise, G. Trombi, and M. Bindi, 2013: Projected shifts of wine regions in response to climate change. *Climatic Change*, **119**, 825–839, doi:10.1007/s10584-013-0739-y.

Nakićenović, N., and Coauthors, 2000: *Emissions Scenarios.* Cambridge University Press, 570 pp.

Nicholas, P., P. Magarey, and M. Wachtel, Eds., 1994: *Diseases and Pests.* Winetitles, 106 pp.

Olson, R., Y. Fan, and J. P. Evans, 2016: A simple method for Bayesian model averaging of regional climate model projections: Application to southeast Australian temperatures. *Geophys. Res. Lett.*, **43**, 7661–7669, doi:10.1002/2016GL069704.

Perkins, S., A. Pitman, N. Holbrook, and J. McAneney, 2007: Evaluation of the AR4 climate models' simulated daily maximum temperature, minimum temperature, and precipitation over Australia using probability density functions. *J. Climate*, **20**, 4356–4376, doi:10.1175/JCLI4253.1.

Pitts, R., and T. Lyons, 1990: Airflow over a two-dimensional escarpment. II: Hydrostatic flow. *Quart. J. Roy. Meteor. Soc.*, **116**, 363–378, doi:10.1002/qj.49711649207.

Räisänen, J., and Coauthors, 2004: European climate in the late twenty-first century: Regional simulations with two driving global models and two forcing scenarios. *Climate Dyn.*, **22**, 13–31, doi:10.1007/s00382-003-0365-x.

Raupach, M. R., P. Briggs, V. Haverd, E. King, M. Paget, and C. Trudinger, 2009: Australian Water Availability Project (AWAP): CSIRO Marine and Atmospheric Research component: Final report for phase 3. CAWCR Tech. Rep. 013, 72 pp. [Available online at http://www.csiro.au/awap/doc/CTR_013_online_FINAL.pdf.]

Reda, A. T., 2015: SMHI-RCA model captures the spatial and temporal variability in precipitation anomalies over East Africa. *J. Climatol. Wea. Forecasting*, **3**, 138, doi:10.4172/2332-2594.1000138.

Roderick, M. L., F. Sun, W. H. Lim, and G. D. Farquhar, 2014: A general framework for understanding the response of the water cycle to global warming over land and ocean. *Hydrol. Earth Syst. Sci.*, **18**, 1575–1589, doi:10.5194/hess-18-1575-2014.

Roeckner, E., and Coauthors, 2003: The atmospheric general circulation model ECHAM 5. Part I: Model description. Max Planck Institute for Meteorology Tech. Rep. 349, 140 pp. [Available online at https://www.mpimet.mpg.de/fileadmin/publikationen/Reports/max_scirep_349.pdf.]

Ruml, M., and Coauthors, 2012: On the use of regional climate models: Implications of climate change for viticulture in Serbia. *Agric. For. Meteor.*, **158-159**, 53–62, doi:10.1016/j.agrformet.2012.02.004.

Rummukainen, M., 2016: Added value in regional climate modeling. *Wiley Interdiscip. Rev.: Climate Change*, **7**, 145–159, doi:10.1002/wcc.378.

Salathe, E. P., L. R. Leung, Y. Qian, and Y. Zhang, 2010: Regional climate model projections for the state of Washington. *Climatic Change*, **102**, 51–75, doi:10.1007/s10584-010-9849-y.

Seguin, B., 2005: Climate warming: Consequences for viticulture and the notion of 'terroirs' in Europe. *Acta Hortic.*, **689**, 61–70, doi:10.17660/ActaHortic.2005.689.3.

Seth, A., and F. Giorgi, 1998: The effects of domain choice on summer precipitation simulation and sensitivity in a regional climate model. *J. Climate*, **11**, 2698–2712, doi:10.1175/1520-0442(1998)011<2698:TEODCO>2.0.CO;2.

Skamarock, W. C., J. B. Klemp, J. Dudhia, D. O. Gill, D. M. Barker, W. Wang, and J. G. Powers, 2005: A description of the Advanced Research WRF version 2. NCAR Tech. Note NCAR/TN–468+STR, 100 pp. [Available online at http://www2.mmm.ucar.edu/wrf/users/docs/arw_v2_070111.pdf.]

Smith, I., P. McIntosh, T. Ansell, C. Reason, and K. McInnes, 2000: Southwest Western Australian winter rainfall and its association with Indian Ocean climate variability. *Int. J. Climatol.*, **20**, 1913–1930, doi:10.1002/1097-0088(200012)20:15<1913::AID-JOC594>3.0.CO;2-J.

Soares, P. M. M., R. M. Cardoso, P. M. A. Miranda, J. de Medeiros, M. Belo-Pereira, and F. Espirito-Santo, 2012: WRF high resolution dynamical downscaling of ERA-Interim for Portugal. *Climate Dyn.*, **39**, 2497–2522, doi:10.1007/s00382-012-1315-2.

Stock, M., F.-W. Gerstengarbe, T. Kartschall, and P. Werner, 2005: Reliability of climate change impact assessments for viticulture. *Acta Hortic.*, **689**, 29–39, doi:10.17660/ActaHortic.2005.689.1.

Taylor, K. E., 2001: Summarizing multiple aspects of model performance in a single diagram. *J. Geophys. Res.*, **106**, 7183–7192, doi:10.1029/2000JD900719.

——, R. J. Stouffer, and G. A. Meehl, 2012: An overview of CMIP5 and the experiment design. *Bull. Amer. Meteor. Soc.*, **93**, 485–498, doi:10.1175/BAMS-D-11-00094.1.

Tonietto, J., and A. Carbonneau, 2004: A multicriteria climatic classification system for grape-growing regions worldwide. *Agric. For. Meteor.*, **124**, 81–97, doi:10.1016/j.agrformet.2003.06.001.

Tóth, J., and Z. Végvári, 2016: Future of winegrape growing regions in Europe. *Aust. J. Grape Wine Res.*, **22**, 64–72, doi:10.1111/ajgw.12168.

Urhausen, S., S. Brienen, A. Kapala, and C. Simmer, 2011: Climatic conditions and their impact on viticulture in the upper Moselle region. *Climatic Change*, **109**, 349–373, doi:10.1007/s10584-011-0059-z.

Wang, W., and Coauthors, 2015: ARW version 3 modeling system user's guide. National Center for Atmospheric Research Tech. Rep., 428 pp.

Webb, L. B., P. H. Whetton, and E. W. R. Barlow, 2007: Modelled impact of future climate change on the phenology of winegrapes in Australia. *Aust. J. Grape Wine Res.*, **13**, 165–175, doi:10.1111/j.1755-0238.2007.tb00247.x.

——, ——, and ——, 2008: Climate change and winegrape quality in Australia. *Climate Res.*, **36**, 99–111, doi:10.3354/cr00740.

Wilby, R., S. Charles, E. Zorita, B. Timbal, P. Whetton, and L. Mearns, 2004: Guidelines for use of climate scenarios developed from statistical downscaling methods. IPCC Tech. Rep., 27 pp. [Available online at https://www.narccap.ucar.edu/doc/tgica-guidance-2004.pdf.]

Wines of Western Australia, 2014: Western Australian wine industry strategic plan 2014–24. Wines of Western Australia Rep., 58 pp. [Available online at http://static1.squarespace.com/static/552d3a93e4b0a7ee3a2ce896/t/555c10ffe4b04aa921b678dc/1432097023899/35368+WINE_Wine+Industry+WA_Strategic+Plan_WEB.pdf.]

Wright, P. B., 1974: Seasonal rainfall in southwestern Australia and the general circulation. *Mon. Wea. Rev.*, **102**, 219–232, doi:10.1175/1520-0493(1974)102<0219:SRISAA>2.0.CO;2.

Wulfmeyer, V., and Coauthors, 2008: The Convective and Orographically Induced Precipitation Study: A research and development project of the World Weather Research Program for improving quantitative precipitation forecasting in low-mountain

regions. *Bull. Amer. Meteor. Soc.*, **89**, 1477–1486, doi:10.1175/2008BAMS2367.1.

Xu, Y., T. Castel, Y. Richard, C. Cuccia, and B. Bois, 2012: Burgundy regional climate change and its potential impact on grapevines. *Climate Dyn.*, **39**, 1613–1626, doi:10.1007/s00382-011-1284-x.

Xu, Z., and Z.-L. Yang, 2012: An improved dynamical downscaling method with GCM bias corrections and its validation with 30 years of climate simulations. *J. Climate*, **25**, 6271–6286, doi:10.1175/JCLI-D-12-00005.1.

Yu, M., and G. Wang, 2014: Impacts of bias correction of lateral boundary conditions on regional climate projections in West Africa. *Climate Dyn.*, **42**, 2521–2538, doi:10.1007/s00382-013-1853-2.

Zhang, Y., V. Dulière, P. W. Mote, and E. P. Salathé Jr., 2009: Evaluation of WRF and HadRM mesoscale climate simulations over the U.S. Pacific Northwest. *J. Climate*, **22**, 5511–5526, doi:10.1175/2009JCLI2875.1.

Zwiers, F. W., and H. von Storch, 1995: Taking serial correlation into account in tests of the mean. *J. Climate*, **8**, 336–351, doi:10.1175/1520-0442(1995)008<0336:TSCIAI>2.0.CO;2.